Degradation of polymer/substrate interfaces – an attenuated total reflection Fourier transform infrared spectroscopy approach

THESIS

Presented in Partial Fulfillment of the Requirements for the Degree Master of Science in the Graduate School of The Ohio State University

By

Arijit Ghosh, B.Sc., M.Sc.

Graduate Program in Chemistry

The Ohio State University

2010

Master's Examination Committee:

Heather C. Allen, Advisor

Joshua E. Goldberger

Gerald S. Frankel

Copyright by

Arijit Ghosh

2010

Abstract

Organic coatings are extensively applied to protect metal structures from corrosion related damage. The durability of such polymer coated adhesively bonded joint structures depends upon the stability of the interfaces between the polymer and the substrate it is coated on. It is economically important to have a thorough understanding of how such interfaces react to a variety of aggressive media that are relevant to real life scenarios.

In this thesis, attenuated total reflection Fourier transform infrared (ATR-FTIR) spectroscopy has been used to detect changes at the interfaces between poly (vinyl butyral-*co*-vinyl alcohol-*co*-vinyl acetate) (PVB) and ZnSe upon exposure to ozone, humidity and UV-B light. Also, the response of PVB-aluminum interfaces to liquid water has been studied and compared with the same for eponol (epoxy resin, diglycidyl ether of bisphenol A)-aluminum interfaces. In the presence of ozone, humidity and UV-B radiation, an increase in carbonyl group intensity was observed at the PVB-ZnSe interface indicating structural degradation of the polymer near the interface. However, such changes were not observed when PVB coated ZnSe samples were exposed to moisture and UV-B light in the absence of ozone showing that ozone is responsible for the observed structural deterioration. Liquid water uptake kinetics for the degraded PVB monitored using ATR-FTIR indicated a degradation of the physical structural organization of the polymer film. Exposure of PVB coated aluminum thin film to de-ionized water showed water incorporation at the interface. There were evidences for

polymer swelling, delamination and corrosion of the aluminum film under the polymer layer. On the contrary, delamination/swelling of the polymer was not observed at the eponol-aluminum interface, although water was still found to be incorporated at the interface. Al-O species were also observed to form beneath the polymer layer. A decrease of the C-H intensities was detected at the PVB-aluminum interface during the water uptake of the polymer, whereas an increase of the C-H intensities was observed for the eponol polymer under these conditions. This is assigned to rearrangement of the macromolecular polymer chains upon interaction with water.

Dedication

This document is dedicated to my parents and friends.

Acknowledgments

I would like to take this opportunity to thank the variety of people who have contributed significantly to the thesis and made it a success. First of all, I would like to thank my advisor, Dr. Heather C. Allen whose expert guidance has led to the realization of this thesis. I would then like to thank Dr. Gerald Frankel (Director, Fontana Corrosion Center) whose periodic comments have immensely helped me improve on the thesis. Next, I would like to acknowledge the constant motivation and encouragement of Dr. Ralf Posner (Department of Materials Science and Engineering) who was my second mentor in this project.

I would then like to extend my heartfelt gratitude to Miss Severine Cambier (Department of Materials Science and Engineering), Mr. Tyler Frank (Undergraduate Researcher), Mr. Larry Antal (Chemistry machine shop), Mr. Tom Kelch (Nanotech West laboratory), Mr. John Sullivan (Chemistry Instrument Support Group), Mr. Alex Champagne (Department of Evolution, Ecology and Organismal Biology), Mr. Mark Andio (Department of Materials Science and Engineering), Dr. Chris Beekman, Dr. Shashi Pathak (University of Southern Missisipi) and the entire Allen group for their support in numerous important aspects related to the project and the thesis. They were always available to help me whenever there were impediments in the way. Thanks to my parents for always being my source of inspiation.

Lastly, I would like to thank the U.S. Army Aviation Applied Tech Directorate for funding this project.

Vita

March 2003 .....Frank Anthony Public School, India

2006.....B.Sc. Chemistry, Jadavpur University, India

2008.....M.Sc. Chemistry, Jadavpur University, India

2008 to present .....Graduate Teaching Associate, Department of Chemistry, The Ohio State University

2008 to present……...Graduate Research Associate, Department of Chemistry, The Ohio State University

Publications

Pal, A. Chowdhury, U.K. Mondal, D. Das, B. Nayak, B. Ghosh, A. Maity, S and Chakraborti, D. *Arsenic burden from cooked rice in the populations of arsenic affected and non-affected areas and Kolkata city in West Bengal*, India Environ. Sci. Technol., 2009, 43 (9), pp 3349-3355

Fields of Study

Major Field: Chemistry

Table of Contents

Abstract ii

Dedication iv

Acknowledgments v

Vita vvii

List of Tables xx

List of Figures x

Chapter 1: Introduction 1

Chapter 2: Instrumentation and Methods 13

2.1 Attenuated Total Reflection Fourier Transform Infrared (ATR-FTIR) Spectroscopy 13

2.2 Ion sputter deposition 18

2.3 The exposure set up 19

2.4 Materials used 20

Chapter 3: Results and Discussion: Degradation of Poly(vinyl butyral) upon exposure to ozone, UV radiation and humidity 30

3.1 Exposure to ozone, UV and moisture 30

3.2 Water uptake kinetics in degraded vs. non-degraded PVB..... 33

3.3 Exposure to UV and moisture..... 35

Chapter 4: Results and Discussion: Water uptake by polymer coated Aluminum-Stability of Aluminum-polymer interfaces……..47

4.1 Water uptake by PVB coated Aluminum..……47

4.2 Water retention at the PVB-Al interface……51

4.3 Water uptake by eponol coated Aluminum……...52

Chapter 5: Conclusions and recommendations……...68

References……71

List of Tables

Table 4.1. Parameters for the pure water OH stretch spectral fits 59

Table 4.2. Parameters for PVB confined water OH stretch spectral fits……..59

Table 4.3. Parameters for eponol confined water OH stretch spectral fits……...65

List of Figures

Figure 1.1.Schematic representation of a coating system.. ……...10

Figure 1.2.Poly (vinyl butyral-*co*-vinyl alcohol-*co*-vinyl acetate) 11

Figure 1.3.Eponol resin 53 BH 35 12

Figure 2.1.Schematic representation of the aluminum-PVB sample configuration showing total internal reflection of the IR beam and generation of evanescent waves 22

Figure 2.2a.Dispersion curve for aluminum b.Variation of IR evanescent wave penetration depths at the aluminum-PVB interface as a function of IR frequency 23

Figure 2.3.Variation of IR evanescent wave penetration depths at the aluminum-eponol interface as a function of Ifrequency……....24

Figure 2.4.Schematic representation of the ZnSe-PVB sample configuration showing total internal reflection of the IR beam and generation of evanescent waves . ……25

Figure 2.5.Variation of IR evanescent wave penetration depths at the ZnSe-PVB interface as a function of IR frequency..... 26

Figure 2.6.Schematic representation of the exposure set up (constructed by Severine Cambier, Frankel Lab) 27

Figure 2.7a.A sample in the cell being exposed to UV-B radiation b.The ozone and humid generation systems (courtesy Severine Cambier)..... …28

Figure 2.8.Spectral emission profile of the Hg UV-B lamp (collected in association with Miss Severine Cambier)…….29

Figure 3.1a.PVB film on a ZnSe IRE **before** exposure to 0.1 ppm ozone, 90% RH and UV-B light b.PVB film on a ZnSe IRE **after** exposure to 0.1 ppm ozone, 90% RH (nitrogen) and UV-B light for 72 hours…….38

Figure 3.2.ATR-FTIR spectrum of PVB spin coated on a ZnSe IRE. The pure ZnSe IRE was used as the background. The spectrum is averaged over 400 scans……...39

Figure 3.3.ATR-FTIR spectra of PVB spin coated on a ZnSe IRE before and after exposure to 0.1 ppm ozone, 90% RH and UV-B (310 nm) radiation for 72 hours. The pure ZnSe IRE was used as the background for both spectra. Each spectrum is averaged over 400 scans. The inset shows the same spectrum zoomed in the region 1500-1800 cm^{-1} to show the intensity increase in both C=O stretch and O-H deformation modes…….40

Figure 3.4.ATR-FTIR spectra of the degraded and non-degraded PVB samples in contact with de-ionized water within 5 minutes of exposure, using pure ZnSe as background and averaged over 128 scans……....41

Figure 3.5.ATR-FTIR spectra of the **degraded** PVB sample showing abrupt water uptake upon exposure to de-ionized water over a period of 2 hours. The degraded polymer was used as the background after drying in a desiccator for 48 hours. Each spectrum is averaged over 128 scans……42

Figure 3.6.IR absorption intensities at 3450 cm^{-1} vs. exposure time for the **degraded** PVB film spin coated on a ZnSe IRE in contact with de-ionized water…….43

Figure 3.7.ATR-FTIR spectra of the **non-degraded** PVB sample showing gradual water uptake upon exposure to de-ionized water over a period of 2 hours. The dry polymer was used as the background. Each spectrum is averaged over 128 scans…….44

Figure 3.8.IR absorption intensities at 3450 cm^{-1} vs. exposure time for the **non-degraded** PVB film spin coated on a ZnSe IRE in contact with de-ionized water……45

Figure 3.9.ATR-FTIR spectra of PVB spin coated on a ZnSe IRE before and after exposure to 90% RH and UV-B (310 nm) radiation for 72 hours. The pure ZnSe IRE was used as the background for both spectra. Each spectrum is averaged over 400 scans. The inset shows the same spectrum zoomed in the region 1500-1800 cm^{-1} to show the intensity increase in the O-H deformation mode only……...46

Figure 4.1.Schematic of an Al-PVB sample exposed to de-ionized water……....55

Figure 4.2.ATR-FTIR spectra of a ZnSe IRE sputter coated with a 50 nm Al film and a 10 μm PVB film in contact with de-ionized water with the dry sample before exposure as background. The exposure times were 1, 3 and 5 hours respectively. Each spectrum is averaged over 400 scans……56

Figure 4.3.ATR-FTIR spectrum of a ZnSe IRE sputter coated with a 50 nm Al film in contact with de-ionized water for 5 hours with the dry sample before exposure as background and averaged over 400 scans……..57

Figure 4.4.Peak fitting of the OH stretch mode of pure de-ionized water. 400 scans were acquired and the pure ZnSe was used as the background……..58

Figure 4.5.Peak fitting of the water OH stretch mode from the 1 hour water exposed aluminum-PVB sample……..58

Figure 4.6.ATR-FTIR spectrum of A ZnSe IRE coated with 50 nm Al and PVB exposed to de-ionized water for 3 hours with the same sample exposed for 1 hour as the background. The spectrum is averaged over 400 scans……60

Figure 4.7.ATR-FTIR spectra of a ZnSe IRE spin coated with a 10 μm PVB film in contact with de-ionized water with the dry sample before exposure as background. The exposure times shown are 5 minutes and 2 hours. Each spectrum is averaged over 400 scans……...61

Figure 4.8.ATR-FTIR spectra of both Al-PVB and PVB samples dried over 48 hours after the water exposure experiments, using the respective dry samples (before exposure) as backgrounds. Each spectrum is averaged over 400 scans…….62

Figure 4.9.Schematic of the possible interactions of water molecules with the Al oxide/hydroxide film at the Al-PVB interface. PVB (right) loses water completely after drying…….63

Figure 4.10.ATR-FTIR spectra of a ZnSe IRE sputter coated with a 50 nm Al film and a 10 μm eponol film in contact with de-ionized water with the dry sample before exposure as background. The exposure times were 1, 3 and 5 hours respectively. Each spectrum is averaged over 400 scans……64

Figure 4.11.Peak fitting of the water band from the 1 hour exposed aluminum-eponol sample……65

Figure 4.12.ATR-FTIR spectrum of a ZnSe IRE sputter coated with a 50 nm Al film and a 10 μm eponol film in contact with de-ionized water for 15 hours with the dry sample before exposure as background, zoomed in the region 2500 – 3700 cm^{-1} showing an increase in the C-H peak intensities and averaged over 400 scans……....66

Figure 4.13.ATR-FTIR spectrum of eponol spin coated on ZnSe and exposed to 90% humid air for 20 hours, using the dry sample before exposure as the background. The spectrum is averaged over 400 scans…….67

Chapter 1

INTRODUCTION

Corrosion of metal structures has been an ever increasing expenditure on almost every nation's economy. Extensive studies conducted by various countries in the world have shown that annual corrosion costs range from 1-5% of the gross national product of each nation.[1] Apart from the economic costs, corrosion can lead to structural damage, thereby posing significant danger to human beings and the surroundings. In the last couple of decades, both inorganic and organic polymeric coatings have been extensively applied on metal structures to prevent corrosion related failures.[2,3] The anticorrosive properties of these coatings (individual components or as a whole) are assessed with the help of certain standard accelerated weathering tests. These studies evaluate the coating's response to UV radiation, humidity, thermal aging, mechanical deformation, electrolytes and water permeation.[4,5]

It is known that most polymers degrade irreversibly due to photolytic oxidation, leading to a concomitant deterioration in their aesthetic and performance parameters.[6] Only wavelengths from approximately 290 nm to 3000 nm are able to reach the troposphere. Wavelengths below 290 nm are strongly absorbed by stratospheric ozone

and other absorbing species in the upper atmosphere. Hence, tropospheric photochemistry is limited by this short wavelength cut off. The UV region is divided into three sub regions, namely UVA (315-370 nm), UVB (290-315 nm) and the more harmful UVC (200-290 nm) which fortunately, is filtered out by ozone. The impact of high energy UV light is the most intense although the contributions from the visible and infra-red wavelengths cannot be fully ignored.[7,8]

The first and foremost criterion for photo-degradation to initiate is that the polymer should be able to absorb UV light. Hence, all aliphatic polymers without chromophores in their structures should ideally have a better photo stability in the terrestrial UV range 295-400 nm than aromatic or unsaturated polymers, but in reality the presence of extraneous substances (added during manufacture) and structural inhomogeneities makes the polymer susceptible to attack.[6,8] Exposure to UV radiation may either lead to changes in the chemical structure of the polymer due to formation of new functional moieties or fragmentation of the cross-linked macromolecules initiating at the weakest centers of the polymer. The number of degradation sites may increase due to transfer of excitation energy to the non absorbing parts of the polymer chains via formation of transient species. Such changes ultimately affect the physical and mechanical properties of the coating negatively.[8] There have been extensive studies on photo-degradation of some of the conventional organic coatings namely alkyd, epoxy, acrylate, polyurethane, and polyester employing electrochemical and spectroscopic (IR and UV-Vis) techniques.[9-12] Also, physical/chemical models have been developed to

link laboratory and outdoor exposure data.[13] Polymer degradation is a complicated process and is contingent on a combination of factors like irradiance, distribution of sunlight, ambient temperature, and dose-response characteristics of the polymer.[14]

In addition to sunlight, coatings are constantly exposed to different environments that range from immersion in water or burial in soil to heavily polluted industrial regions.[2] In urban areas with numerous pollution sources, ozone is a major pollutant in the atmosphere. Although stratospheric ozone protects all living beings on the earth from the detrimental UV radiation of the sun, ozone in the troposphere may cause damage to living tissues and degrade numerous materials.[15] Tropospheric ozone concentrations show heterogeneity since it is formed from a series of photochemical reactions involving volatile organic compounds and oxides of nitrogen whose emissions vary geographically, temporally and altitudinally. Also, there is influx of ozone from the stratosphere at times. Ozone concentrations in the range 30-40 ppb are essentially found worldwide. Industrial zones have been found to have 100-150 ppb of ozone. In conjunction with the appropriate UV wavelengths and moisture, ozone is known to undergo numerous photochemical reactions that result in the formation of highly reactive intermediates, which in turn, initiate polymer degradation.[7] Hence, it is very important to have a thorough knowledge of the degradation pathways of polymers upon exposure to these agents to understand their performance abilities better.

Figure 1.1 depicts a schematic representation of a multilayer coating on a metal surface for corrosion protection. Primer layers are very important functional

components of coatings providing a corrosion resistant barrier to the metal surface. They are typically 10-20 μm in thickness and promote adhesion between the topcoat and the surface to be painted. They are responsible for improving paint durability thereby providing extra protection to the material being painted.[16] The performance of the primer is one of the determinants of the performance of the coating as a whole. Topcoats are chosen primarily based on their barrier properties since they serve as the first line of defense to the entering deteriogens. However, they also contain the pigments and additives necessary for aesthetic purposes..

Poly (vinyl butyral-*co*-vinyl alcohol-*co*-vinyl acetate) or simply poly (vinyl butyral) (PVB) is a non toxic polymeric resin known for its fine properties like transparence, insulation, impacting resistance and drawing performance.[17] The chemical structure of PVB is shown in Figure 1.2. It can be synthesized by a condensation reaction of butyraldehyde and poly (vinyl alcohol) using N-methyl-1-pyrrolidone as solvent.[18] It exhibits special adhesiveness and transparence to both organic and inorganic glass, for which reason it is extensively used in laminated safety glass for automobile windshields.[19] However, PVB is also applied as primers in multi-layered coating systems for corrosion protection of metal structures.[17] There has been a lot of research on thermal and photo-chemical degradation of PVB using gravimetric and spectroscopic methods. According to studies by Nabil M. et al. [20], thermal degradation in PVB initiates at the acetate group. Liau et al. [21] investigated the effect of 380 nm on the structure of PVB and

found that under normal conditions, there is no photo-degradation of the polymer but addition of TiO_2 enhanced the photo-deterioration process. However, the most realistic approaches related to real-life scenarios would include exposure of PVB to different combinations of ozone, UV light and humidity (resembles an industrial environment) rather than heat or light alone.

In addition to understanding what factors are responsible for polymer failure and the degradation mechanisms, it is important to know whether the exposure of PVB coated substrates affects the polymer/substrate interface in a similar manner compared to the polymer bulk structure. Adhesively bonded structures seen everywhere today can be simply considered to be polymer coated substrates, whose longevity depends upon the stability of the polymer/substrate interfaces. Common substrates employed are metals and alloys due to their desirable properties like tensile strength and luster. Hydration and structural changes are known to be detrimental to such interfaces. This is also very likely because a polymer/substrate interface is often a fragile region with inferior properties compared to the material bulk.[22] Metal-polymer interfaces are known to be fractal in nature and not smooth microscopically.[23] The structure of the metal oxide layer plays a crucial role in determining the initial integrity of the polymer/metal bonds and the bonding has been found to change with variations in temperature.[23,24] One of the factors affecting the deterioration of such interfaces is coating to metal adhesion. Several different theories of adhesion between polymers and substrates have been proposed, namely the physical adhesion theory, where Van der Waals/dispersion interactions are

operative, the chemisorption theory which involves the formation of covalent, ionic or hydrogen bonds at the interface, the diffusion theory involving inter-diffusion of the polymer into the substrate bulk, the mechanical interlocking theory where the polymer chains anchor themselves into surface defects of the substrate and the weak boundary theory which states that absence of contaminants promote polymer-substrate adhesion.[25,26] Another factor is the barrier properties of the polymer film to oxygen and water, which are also ingredients of metal corrosion.[22]

Water is the most abundant substance on Earth. If the activity of water is higher in the environment compared to the polymer coated metal structure, it would spontaneously diffuse into the polymer network through pores or defects, and ultimately reach the polymer/metal interface, where it is known to cause adhesion loss between the polymer and the metal surface by displacing the weaker polymer/metal bonds by stronger water/metal oxide-hydroxide interactions.[27] It is possible that the hydrophilic metal oxide/hydroxide surface may retain the water molecules at the buried polymer/metal interfaces over a period of time. In addition, the penetrating medium often results in an adjustment of the bulk structure of the polymer film, too. This includes reversible swelling, irreversible hydrolysis, cracking, and crazing.[22] Severe changes in the physical properties of the resin are observed, such as tensile strength, net dielectric constant, and the glass transition temperature.[28] The ultimate impact can be delamination or stripping of the film from the metal surface. These complex processes are contingent on the

structure and chemical properties of the polymer film (polarity, unsaturation, symmetry, chain orientation etc.), as well as size, shape and properties of the penetrant species.[29]

Aluminum is a low density metal with good mechanical strength. It is extensively used in outdoor applications that include siding, window trim, automotive elements and aircrafts. Also, the recent demand to reduce the use of fossil fuels has led to an increased interest in lightweight constructions like Al alloys.[30,31] Hence, it is extremely crucial that adhesively bonded structures using aluminum last a long time. In this context, a PVB coated aluminum surface can be used as a model system to investigate how the corresponding polymer-metal interface responds to the ingress of water and how effective is PVB in protecting the metal beneath it. Also, a comparison with an epoxy polymer-aluminum interface (epoxies are well known primer resins.[2]) is helpful. The epoxy resin used was eponol resin 53 BH 35 and is based on Di-glycidyl ether of Bisphenol A (DGEBA). The structure of the resin is shown in Figure 1.3.

Probing changes at buried interfaces non-destructively have always been challenging to scientists. One of the potential limitations is that the technique should work at ambient pressure as applying a high vacuum might cause severe alterations of the surface. Moreover, real time analysis and relevant climatic conditions are always desired. There have been numerous studies on water sorption by polymeric coatings using gravimetric procedures, which, however do not shed light on the polymer/metal interfacial region specifically.[32,33] Commonly employed methods so far in determining changes at such interfaces are electrochemical techniques, for example electrochemical

impedance spectroscopy (EIS) or the scanning Kelvin probe (SKP). While EIS is used to analyze the resistive and capacitive barrier properties of the polymer coating and the polymer/metal interface based on electric equivalent circuits, SKP functions by measuring local electrode potential changes beneath the polymer layer.[31,34-36] Spectroscopic techniques have been employed to understand penetrant diffusion through coatings under a variety of conditions.[37,38] However, there is still a lack of detailed knowledge about polymer/metal interfaces using this technique. As examples, Ohman et al. have studied the transport of water and electrolyte species to aluminum-polymer interfaces and Nguyen et al. investigated the incorporation of water at iron-polymer interfaces, additionally quantifying the amount of water trapped at such interfaces.[22,27, 31,39,40]

In this thesis, a study of the response of PVB resin (PVB-ZnSe interfaces) to ozone, relative humidity and ultraviolet radiation and that of aluminum-PVB interfaces to liquid water using attenuated total reflection Fourier transform infrared (ATR-FTIR) spectroscopy is presented. Chapter 2 introduces the theory behind total internal reflection, the working principle of ATR-FTIR spectroscopy and a discussion on the relevance of the technique to this study, in addition to the other tools and sample preparation methods used for the experiments. Chapter 3 focuses on the assessment of the degradation pathways of PVB upon exposure to ozone, humid air and UV-B light. Relevant ATR-FTIR spectra have been presented. An attempt has been made to understand which component(s) is (are) responsible for the structural deterioration of the polymer. The

response of PVB-aluminum interfaces to water has been studied in situ in Chapter 4. Water incorporation, polymer swelling, delamination and corrosion products formation at the interface are some of the areas investigated. Also, a comparison with an eponol (epoxy resin)-aluminum interface is presented. Chapter 5 reports a summary, conclusion and future work recommended on the studies presented in this thesis.

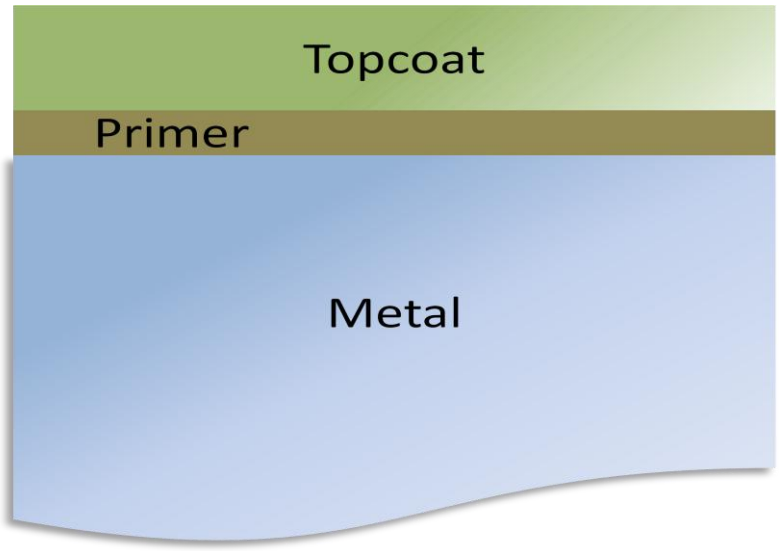

Figure 1.1.Schematic representation of a coating system

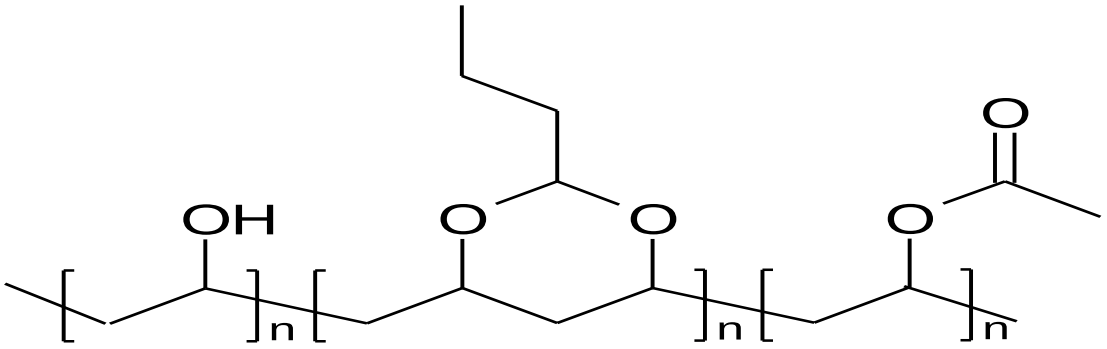

Figure 1.2.Poly (vinyl butyral-*co*-vinyl alcohol-*co*-vinyl acetate)

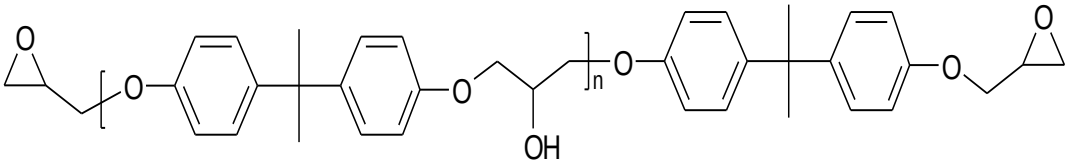

Figure 1.3.Eponol resin 53 BH 35

Chapter 2

INSTRUMENTATION AND METHODS

2.1 ATTENUATED TOTAL REFLECTION FOURIER TRANSFORM INFRARED (ATR-FTIR) SPECTROSCOPY

ATR-FTIR spectroscopy is based on the phenomenon of total internal reflection and the generation of evanescent fields at an internal reflection element (IRE)/sample interface. An electromagnetic radiation travelling from a medium with a higher refractive index (n_1) to a medium with a lower refractive index (n_2) is found to totally internally reflect in the incident medium if the incidence angle of the beam exceeds a certain value, known as the critical angle (Θ_c), and is given by Eqn. 2.1[41],

$$\Theta_c = \sin^{-1} (n_2/n_1) \quad (2.1)$$

In ATR-FTIR spectroscopy, the sample to be analyzed is held in contact with an internal reflection element with a higher refractive index than the sample. An IR beam is then incident on to the IRE (through the IRE bulk) at an angle greater than the critical angle for the particular IRE/sample pair. The total internal reflection creates an evanescent wave that extends beyond the surface of the crystal into the sample held in

contact with it. The evanescent wave can be described as a standing wave, whose field amplitude decays exponentially with distance as given by Eqn. 2.2[41,42],

$$E = E_o \exp[-\gamma z] \quad (2.2)$$

Where E is the amplitude in the sample at depth z, γ is a constant and E_o is the amplitude at the sample surface (z=0).

The evanescent wave will be altered in intensity in regions of the IR spectrum where the sample absorbs energy. The attenuated energy from the wave is returned to the IR beam, which then exits the opposite end of the crystal to the detector in the IR spectrometer. The system then generates an IR spectrum.[42] There are numerous IREs available with different refractive indices like ZnSe, silicon, germanium, and diamond among others. It is important to ensure an intimate contact between the sample and the crystal. Both single reflection and multi reflection systems are available, the latter allowing more than one region to be sampled and hence giving an increased signal intensity than the former.

The depth of penetration d_p is a measure of the depth into the surface of the sample that the radiation penetrates and that the resultant spectrum represents, and is given by Eqn. 2.3[41],

$$d_p = \frac{\lambda}{2\pi n_1 (\sin^2\theta - (n_2/n_1)^2)^{1/2}} \quad (2.3)$$

Where λ is the wavelength of the incident radiation, θ is the incidence angle, n_1 and n_2 are the refractive indices of the IRE and the sample respectively. d_p is a good estimate of the depth that is probed in ATR-FTIR experiments, since it is the depth from which majority of the information comes from. However, it is important to understand that the spectral information obtained from ATR-FTIR spectroscopy is the average over the wave that is decaying exponentially with the distance from the surface, and hence, can be considered to be composed of decreasing contributions from the deeper layers in the sample as d_p is approached. This evanescent field penetration depth is usually in the nanometer or low micrometer range.[41]

As can be seen from Eqn. 2.3, the penetration depth is directly proportional to the wavelength of the incident radiation. Due to the fact that transmission IR spectroscopy probes both the interface and the polymer bulk structure, ATR and transmission spectra for the same sample are different.[41] ATR-FTIR spectra may show band distortions which are attributed to changes in reflectivity at different interfaces due to interference by the real part of the complex refractive index.

With the help of ATR-FTIR spectroscopy, both qualitative and quantitative analyses of samples can be carried out over wide spectral ranges and with little sample preparation.[43] Also, the ATR technique is useful for analyzing thick samples having high absorption coefficients, because normal transmission IR spectroscopy would fail under such circumstances due to the longer path length of the IR beam through the strongly

absorbing sample. The primary advantage of ATR-FTIR is that it allows investigation of surfaces and interfaces whereas the major signal contribution for conventional transmission and external reflection IR techniques results from the probed bulk structures. Chemical composition, layer structure, diffusion, adsorption, chemical reaction monitoring, orientation and physical state of surfaces are a few types of analyses that can be accomplished by ATR-FTIR.[41] It is also possible to track changes at interfaces as a function of time upon the sample's exposure to IR active species. Philippe et al.[44] have computed water sorption and desorption transport coefficients of water and inhibitor inorganic ions in a series of epoxy resins using ATR-FTIR spectroscopy. Similar water diffusion studies were also done by Fieldson et al.[45] The aggregation states of penetrant species inside polymers have also been studied using this technique.

Figure 2.1 shows the sample configuration for the PVB-aluminum experiments. The sample comprises an approximately 10 μm thick PVB layer spin coated on a 50 nm aluminum film, which is sputter coated on a ZnSe IRE. The refractive index of Al varies from 3.38 at 4000 cm^{-1} to 43.43 at 650 cm^{-1}, while those for ZnSe and PVB are 2.40 (2.44-2.37, average is 2.40) and 1.48 respectively and can be considered constant within the above mentioned frequency range.[46,47] The dispersion curve for aluminum is shown in Figure 2.2a. Therefore, the IR beam would suffer total internal reflection at the Al-PVB interface and not at the ZnSe-aluminum interface according to the first criterion of total internal reflection. The critical angles of the IR beam at the aluminum-PVB interface would vary significantly over the probed IR region since the refractive index of

Al changes in this range. The critical angles were calculated using equation 2.1, and were found to be 27˚ at 4000 cm^{-1} and 2˚ at 650 cm^{-1}. Now, in agreement with the Snell's law of refraction, the incident angles of the IR beam were found to exceed the above mentioned critical angles, and this holds for every wavelength of the investigated range. At 4000 cm^{-1}, the IR incident angle was found to be 30˚ (critical angle is 27˚) and at 650 cm^{-1}, it was 2.2˚ (critical angle is 2˚). This satisfies the second criterion for the total internal reflection phenomenon. Hence, a small region in close proximity to the aluminum-PVB interface was probed. Figure 2.2b shows the variation of the evanescent wave penetration at the aluminum-PVB interface in the investigated frequency region. Similarly, for the experiments involving aluminum-eponol interfaces, the variation of the evanescent field depth with frequency can be calculated using DGEBA's refractive index, which is 1.57.[48] Figure 2.3 shows the corresponding penetration depth vs. frequency plot. Similar to the aluminum-PVB samples, the aluminum-eponol interface was probed using ATR-FTIR spectroscopy.

For the experiments involving PVB only, Figure 2.4 represents the sample configuration which is an approximately 10 μm thick PVB film spin coated on a ZnSe IRE. Here again, ATR-FTIR spectroscopy is the most appropriate tool to investigate changes close to the PVB-ZnSe interface. Figure 2.5 shows how the penetration depth of the evanescent field changes across the IR frequency range.

A Thermo Nicolet FTIR spectrometer (Avatar 370, Thermo Electron Corporation) that uses a DTGS detector was employed for the ATR-FTIR experiments. A 45° single bounce ZnSe internal reflection element (20 mm diameter, 3 mm thickness,

7002-402, Smiths Detection Ltd.) trough ATR accessory (Smart SpeculATR, Thermo Electron Corporation) was used to collect the spectra at a spectral resolution of 4 cm^{-1}. The spectra were averaged over 400 and 128 scans (as specified below respective spectra).

2.2 ION SPUTTER DEPOSITION

Ion sputter deposition is a method of thin film preparation that involves physical vaporization of atoms from a surface due to momentum transfer from bombarding energetic atom-sized particles. This method is extensively applied for preparing metallic, resistive and conducting films. The energetic particles are usually ions of a gaseous substance accelerated in an electric field.[49] There are three sequential stages in the thin film making procedure: evaporation (or sputtering) of the substance creating an atomic beam; transport of this atomic beam in space from the target to the substrate; and condensation of the atoms on to the substrate forming the film.[50] Thin film preparation by physical vapor deposition is a very complicated process in the sense that it takes intensive knowledge to be able to produce superior quality films. The film quality depends on a number of factors such as temperature of evaporation, the atomic beam intensity, and gas pressure in the chamber or the deposition rate.[50] Using aluminum thin films was the best option for this study with ATR-FTIR spectroscopy as the employed analytical tool, primarily because the interfaces between the polymer and aluminum plates or other macroscopic structures cannot be probed using the ATR technique.

Moreover, polymer coated thin films provide the required interface for investigation and this approach has been used by other research groups[22, 27, 31,39, 40].

For the ATR-FTIR measurements with the PVB-aluminum and eponol-aluminum samples, an ATC ORION 5 UHV sputtering system (AJA International, Inc.) was used to deposit the aluminum thin films on ZnSe IREs, with a base working pressure of 5 mTorr. The base pressure was 10^{-7} Torr. A 20 sccm (standard cubic centimeter per minute) flow of Argon was used as the bombarding gas. A deposition rate of 0.8 Angstrom per second was achieved by applying 250 W to the aluminum target. The time required to deposit 50 nm films was initially calculated by depositing a film directly on to a quartz crystal microbalance located inside a vacuum chamber exactly at the same distance from the target as the ZnSe IRE. Keeping all the conditions same, the sensor was then replaced by the ZnSe crystal and deposition was done for the same time.

2.4 THE EXPOSURE SET UP

Exposure of the PVB samples were carried out in a custom made set up, designed and constructed by Severine Cambier (Frankel lab, Department of Materials Science and Engineering), that allowed the passage of optimum levels of ozone, moist air and UV-B radiation through a cell housing the sample. Figure 2.6 provides a schematic representation of the entire exposure set up. The set up consists of four major parts: the humid air generator, the ozone generator, the sample cell and the UV-B lamp. The humid air generation system uses a nitrogen cylinder to bubble nitrogen gas through two wash bottles filled with de-ionized water. A by-pass around the wash bottles is used to mix dry

nitrogen with the humid one in proportions required to maintain the desired humidity level, as given by a hygrometer (Testo model 610) placed inside the cell. For the ozone generation system, dry oxygen gas from a cylinder is passed through an ozone generator (Jelight model 600) and the emitted ozone concentration is determined with the help of an ozone monitor (Teledyne instruments, Model 465L) placed at the end of the set up. The ozone level is controlled by changing the oxygen flow rate using a mass flow controller (Omega FMA5400/5500). The humid air and ozone flows are merged and directed into a leak proof glass cell with a quartz (UV transparent) cover housing the samples. The cell is placed directly under a UV-B Hg lamp (USHIO G15T8E). Figures 2.7 a and b show pictures of the exposure set up. The distance between the sample surface and the lamp was approximately 6 inches. The spectral emission profile of the Hg lamp is shown in Figure 2.8. For all the experiments, a 90% relative humidity (RH) was maintained by combining humid air at a flow rate of 1.3 standard cubic feet per hour (scfh) with dry air at a rate of 0.2 scfh, whereas to obtain a 0.1 ppm (100 ppb) of ozone, the oxygen flow rate employed was 0.4 scfh. A total flow of 1.7 scfh was passed through the cell per hour.

2.5 MATERIALS USED

Poly (vinyl butyral-*co*-vinyl alcohol-*co*-vinyl acetate) resin (average M_w 70,000-100,000) was purchased from Sigma-Aldrich (Product number 418439-250G). For film preparation by spin coating, 1.5 g of the polymer powder was dissolved in 18.5 g of 99% methanol (Fisher Scientific) and stirred overnight with a magnetic stirrer. Polymer films were then spin-coated from the solution on to the ZnSe IREs (with and

without Al films) at 200 rpm for 5 minutes using a spin coater (TC100, MTI Corporation). The film thickness was determined to be approximately 10 μm as found by a thickness gauge (Elcometer 456, standard used 49.8 microns). The samples were allowed to dry overnight in an evacuated desiccator to let the methanol evaporate. The PVB samples were then exposed in the set up to ozone, RH and UV-B whereas the aluminum-PVB samples were exposed to de-ionized water followed by acquisition of ATR-FTIR spectra. Background spectra were obtained for both samples before film deposition and after film preparation before exposure. For the experiments with the epoxy polymer, Eponol^{TM} resin 53-BH-35 was kindly provided by Hexion Specialty Chemicals. The viscous resin was diluted with a 75/25 wt% solution of methyl ethyl ketone and propylene glycol methyl ether followed by overnight stirring. Thin films were then spin cast from the solution on to a ZnSe IRE (previously coated with a 50 nm aluminum film) using the above mentioned spin coater at 120 rpm for 5 minutes, which generated a film thickness of 8-9 μm as measured by a surface profilometer (Dektak 3). The samples were cured at 160˚C for 12 hours to ensure complete evaporation of the solvents and were then exposed to de-ionized water for acquiring ATR-FTIR spectra. Double distilled de-ionized water was used for all experiments.

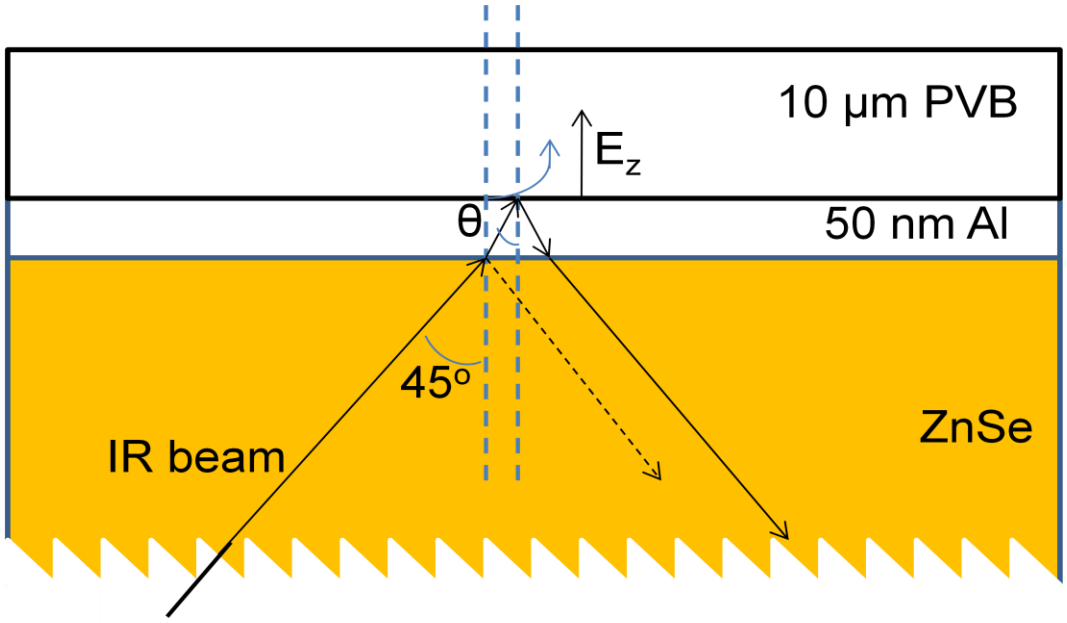

Figure 2.1 Schematic representation of the aluminum-PVB sample configuration showing total internal reflection of the IR beam and generation of evanescent waves

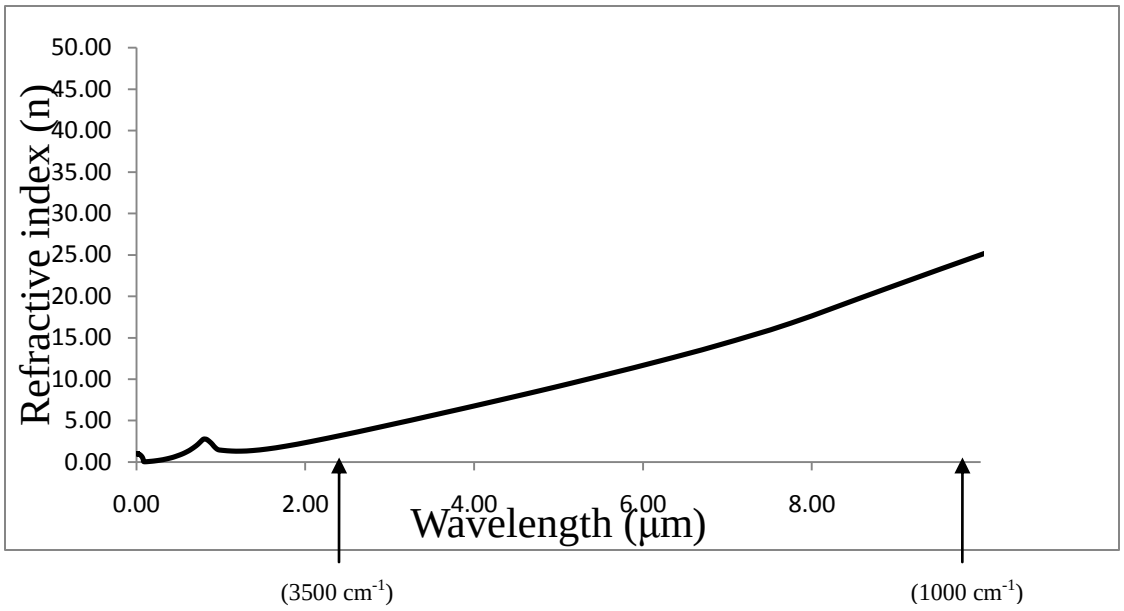

a

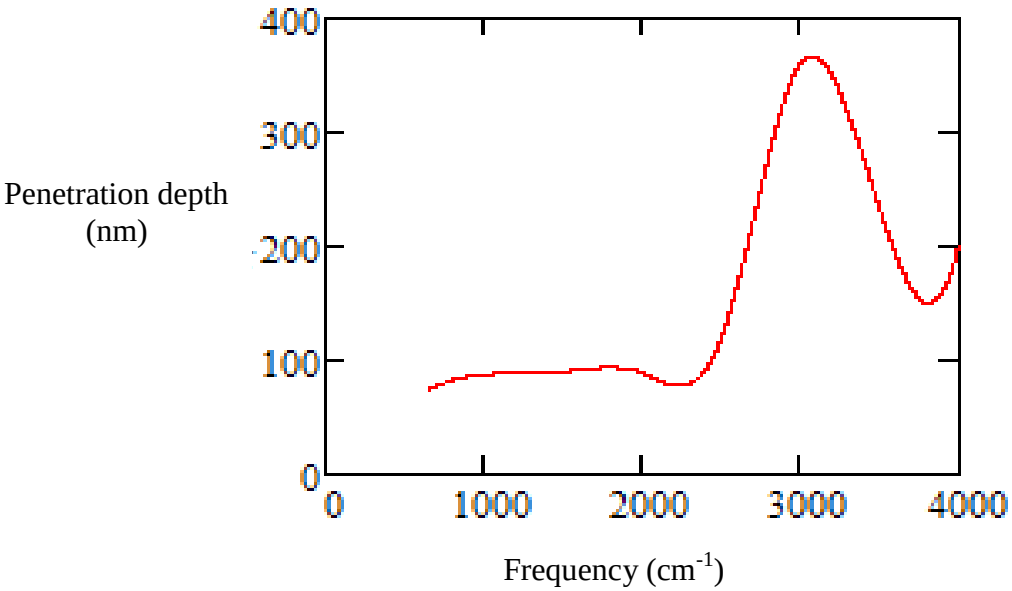

b

Figure 2.2a.Dispersion curve for aluminum **b**.Variation of IR evanescent wave penetration depths at the aluminum-PVB interface as a function of IR frequency

)

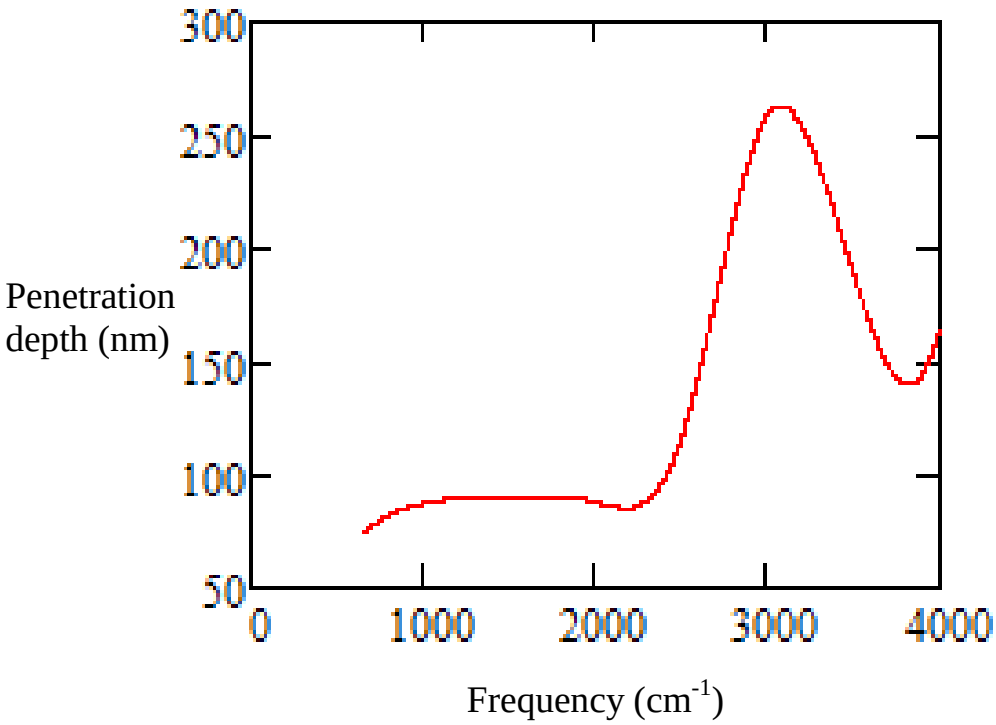

Figure 2.3.Variation of IR evanescent wave penetration depths at the aluminum-eponol interface as a function of IR frequency

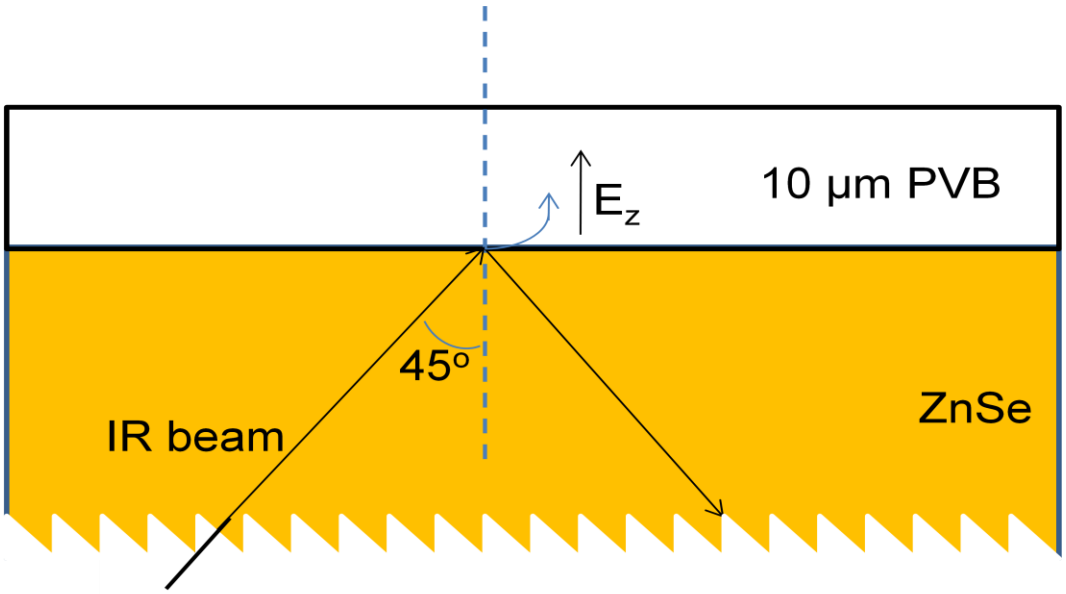

Figure 2.4.Schematic representation of the ZnSe-PVB sample configuration showing total internal reflection of the IR beam and generation of evanescent waves

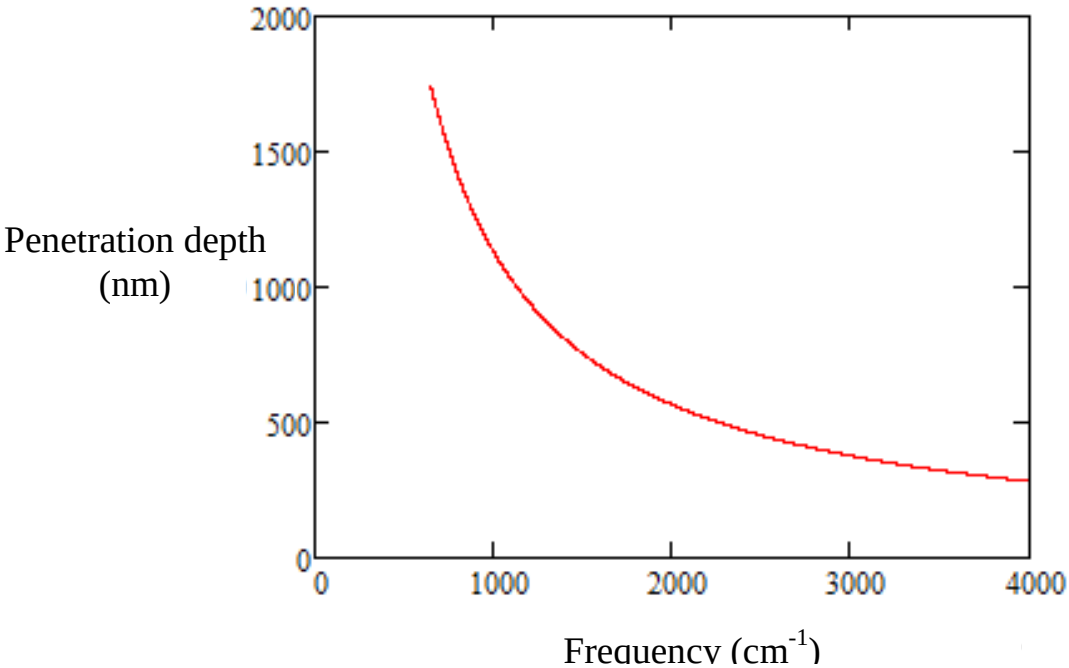

Figure 2.5.Variation of IR evanescent wave penetration depths at the ZnSe-PVB interface as a function of IR frequency

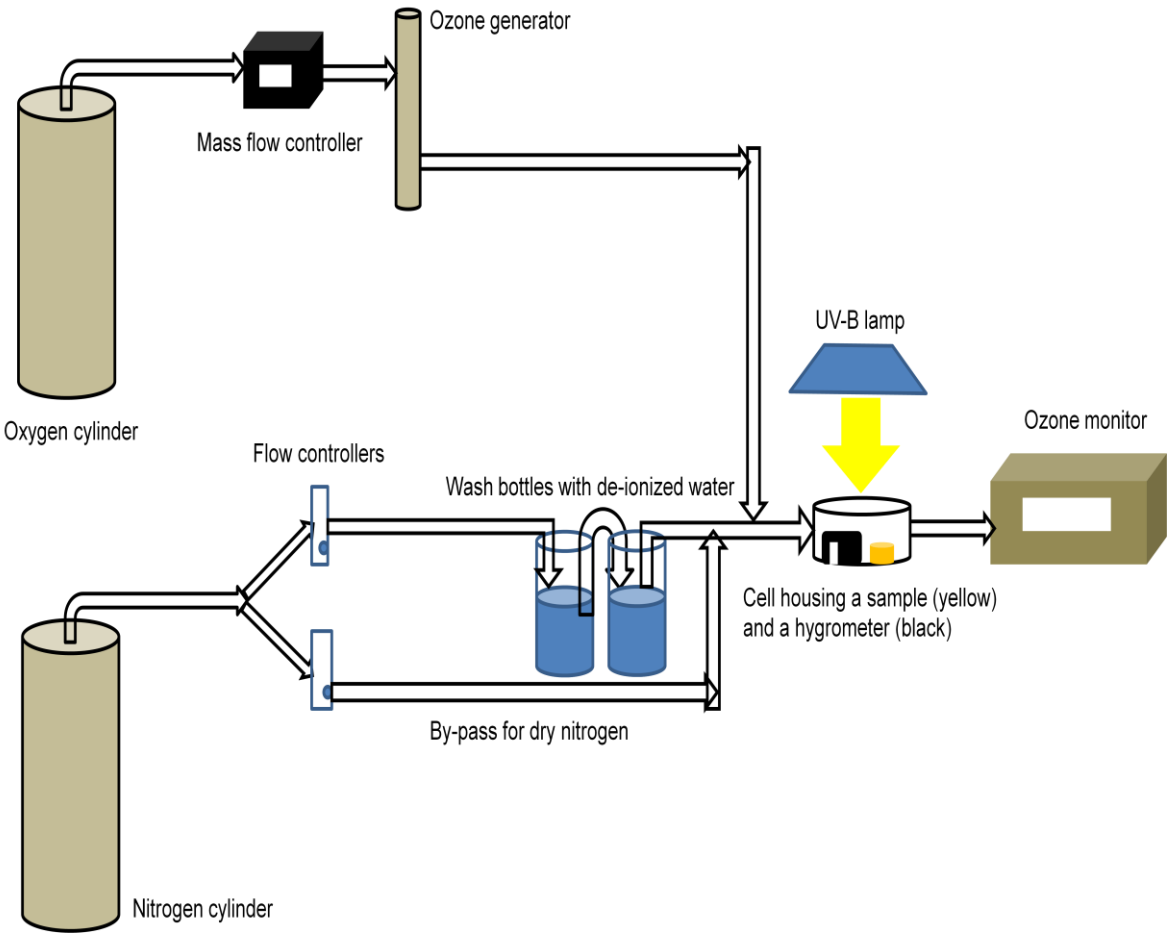

Figure 2.6.Schematic representation of the exposure set up (constructed by Severine Cambier, Frankel Lab)

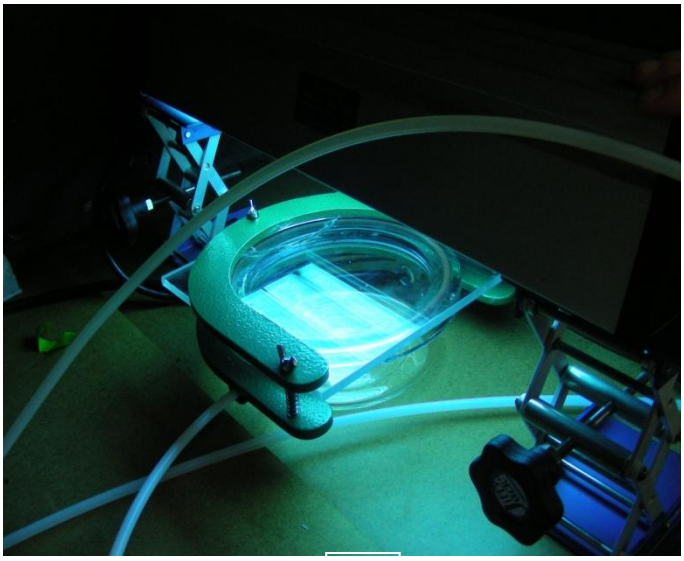

a

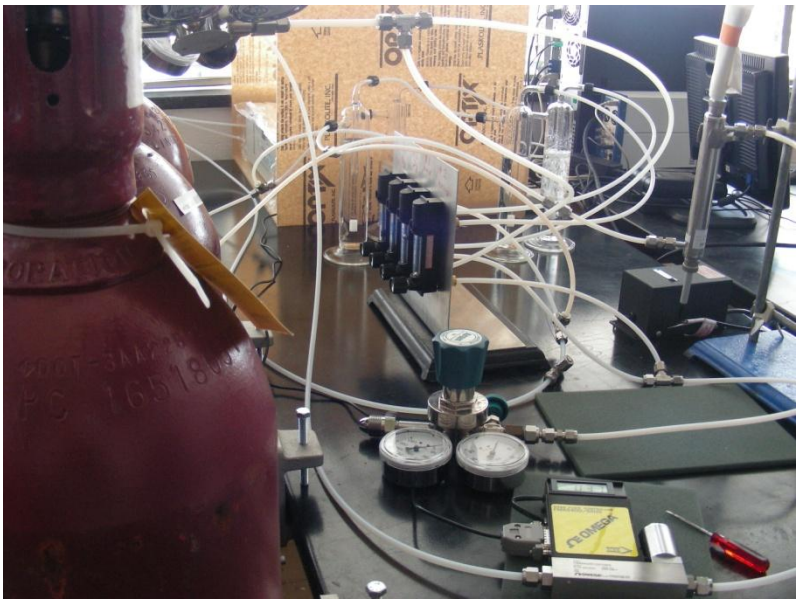

b

Figure 2.7a. A sample in the cell being exposed to UV-B radiation **b** The ozone and humid generation systems (courtesy Severine Cambier, Frankel Lab)

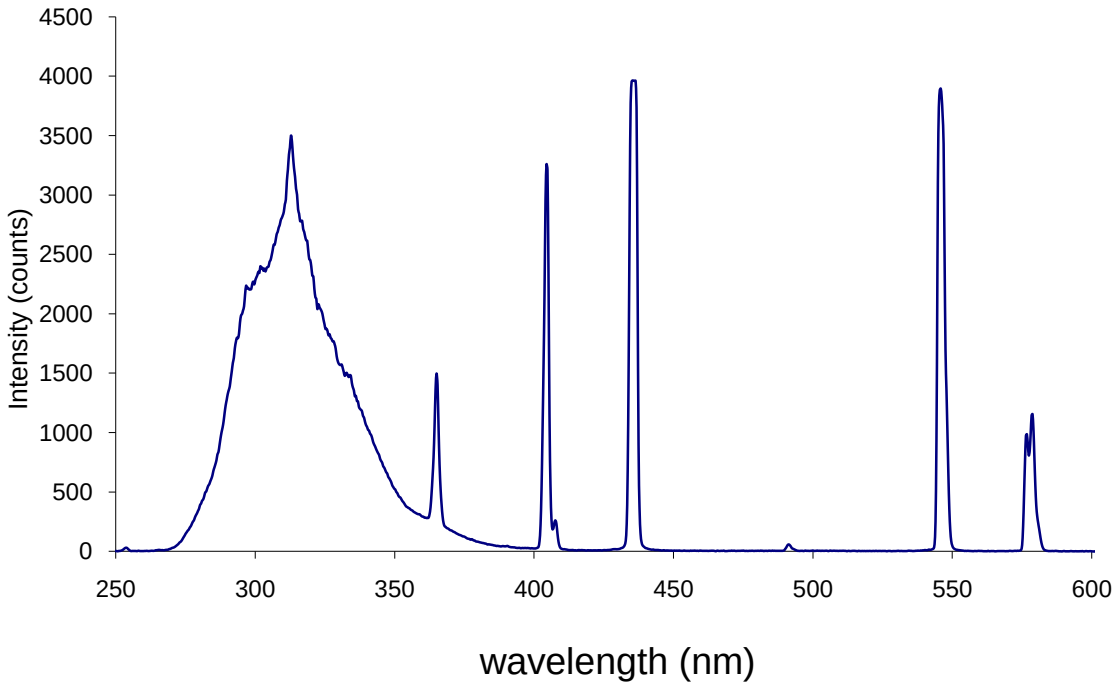

Figure 2.8.Spectral emission profile of the Hg UV-B lamp (collected in association with Severine Cambier, Frankel Lab).

Chapter 3

RESULTS AND DISCUSSION: DEGRADATION OF POLY(VINYL BUTYRAL) UPON EXPOSURE TO OZONE, UV RADIATION AND HUMIDITY

3.1 EXPOSURE TO OZONE, UV AND MOISTURE

With the aim of understanding the degradation pathways of PVB, the PVB coated ZnSe crystals were exposed to 90% RH, 0.1 ppm ozone and UV-B radiation for 72 hours. Figures 3.1 a and b show the physical appearance of the PVB film before and after exposure respectively. It is very clear that the exposed sample appears different from the unexposed one and shows numerous defects across the polymer surface.

Before beginning with the exposure experiments, an ATR-FTIR spectrum of PVB spin coated on a ZnSe IRE was collected. Figure 3.2 shows the above mentioned spectrum. The pure ZnSe crystal was used as the background. The absorption peak at 1000 cm^{-1} can be attributed to the C-OH stretching vibration of PVB. The peaks at 1140 cm^{-1} and lower frequencies primarily correspond to the C-O-C backbone while those in the range 1250-1735 cm^{-1} are due to C=O vibrations and the alcoholic O-H deformation modes of the polymer. The bands in the range 2800-3000 cm^{-1} are assigned to symmetric and asymmetric C-H bond stretches. The O-H stretching modes of the OH moieties of the polymer can be seen at 3450 cm^{-1}.[51] However, the broad band shape of the 3450 cm^{-1}

peak indicates a certain extent of hydrogen bonding between the O-H moieties within the polymer chains. The broad shape is attributed to different hydrogen bonding environments that the O-H moieties reside in the medium, for example, a hydroxyl group bonded to two hydrogen bonds will vibrate at a higher frequency than that bonded to three hydrogen bonds. Hence, there is a distribution of intensities in the frequency range 3000-3700 cm^{-1} based on such environments that broaden the peak. Free O-H groups resonate at the same frequency. Hence, absence of hydrogen bonding is characterized by narrow/sharp peaks.[52]

Figure 3.3 shows the ATR-FTIR spectra of PVB before and after the above mentioned conditions. The pure ZnSe crystal was used as the background. As can be seen, there are four prominent changes in the spectrum before and after exposure. Firstly, the absorption peak at 3450 cm^{-1} was found to increase in intensity. This is due to the ingress of water into the polymer matrix.[53] However, there may be contribution from water formed within the polymer due to the exposure since it is known to be a degradation product of PVB generated by dehydration of the vinyl alcoholic groups of the polymer.[54] Secondly, there is an increase in the 1640 cm^{-1} peak intensity. This is due to the O-H deformation mode of water. Again, there may be contribution from C=C vibrations because dehydration of the alcoholic groups leads to the formation of double bonds in the polymer chain. Butenal is also known to be a degradation product of PVB.[54] The OH bending modes of alcohols appear in the region 1420-1330 cm^{-1} and does not contribute to the 1640 cm^{-1} band.[55] This shows that exposure to 90% RH for 72 hours

leads to incorporation of water in the PVB film in close proximity to the PVB-substrate interface (since the evanescent field penetration depth is about 300 nm at 3450 cm^{-1} for the PVB-ZnSe interface, Figure 2.5) as well as generation of water as a degradation product. Thirdly, the inset of Figure 3.2 also shows the appearance of an absorption band at about 1580 cm^{-1}. This is assigned to the COO^- stretch[55] and is likely due to all the carboxylate species that are generated in the polymer matrix after oxidation by ozone. However, further investigation of this peak is required.

Lastly, there was an increase in intensity of the absorption peak at 1735 cm^{-1}, which is attributed to the C=O stretching mode.[56] Again, this change can be prominently seen in the inset figure, which zooms on the 1500-1800 cm^{-1} region. This hints to a structural change in the polymer film upon exposure to the combination of ozone, humidity and UV-B radiation. Also, the fine structure superimposed on the absorption bands can be attributed to the rotational transitions of water molecules in the vapor phase. IR radiation has sufficient energy to excite rotational transitions whose energies are much smaller than that of vibrational transitions. As a matter of fact, rotational levels are significantly populated even at room temperature (at room temperature, $kT \approx 200\ cm^{-1} >$ rotational energy levels).

Before discussing the possible pathways that might lead to the formation of carbonyl groups, it is important to understand the chemistry unleashed when ozone, humid air and UV-B light are brought together. It is well known that exposure of ozone to UV radiation leads to its photolysis resulting in the formation of both atomic and

molecular oxygen. Either or both of these two can be in electronically excited states depending upon the incident energy. UV energy of 310 nm wavelength has been found to generate two distinct states of O and O_2, as shown by Eqn. 3.1 below,

$$O_3 + h\nu\ (310\ nm) \rightarrow O_2\ (^1\Delta_g) + O\ (^1D) \quad (3.1)$$

The O (^{1}D) formed is highly reactive and can react with water, as shown by Eqn. 3.2 below,

$$O\ (^1D) + H_2O \rightarrow 2OH \quad (3.2)$$

These reactive species are known to attack organics initiating chain reactions.[7] According to studies by Reinohl [57], the tertiary hydrogens present in the PVB structure are the most vulnerable sites of radical attack and yields hydro peroxides in the presence of atomic and/or molecular oxygen.. The latter cleaves easily, either by light or heat, to yield oxygen centered radicals. Liu et al. [58] has shown that such oxygen centered radicals facilitate ring opening and finally, formation of molecular fragments with carbonyl groups. This is probably the reason for the C=O intensity increase in this case. Moreover, thermal oxidative and photochemical degradation of PVB studied by several groups have been found to yield carbonyl products through ring opening and chain scission.[56-59]

3.2 WATER UPTAKE KINETICS IN DEGRADED VS. NON-DEGRADED PVB

To understand if such an exposure had an effect on the physical structural organization of the polymer film, the degraded PVB sample was dried overnight to drive all of the excess water away and then exposed to de-ionized water with the aim of monitoring the water uptake kinetics using ATR-FTIR spectroscopy. This was compared with the water uptake by an unexposed PVB sample, which was dried overnight as usual (to drive the excess methanol away). The aim was to see if the degraded polymer became less resistant to water compared to the intact polymer. Figure 3.4 shows the ATR-FTIR spectra of the degraded and non-degraded PVB samples in contact with de-ionized water within 2 minutes of exposure. The pure ZnSe was taken to be the background. As can be seen from the intensities (peak areas) of the 3450 and 1640 cm^{-1} absorption peaks, the degraded sample shows a significantly greater water uptake than the intact polymer. On the other hand, the absorption bands corresponding to C-H, C-OH, C-O-C stretch intensities were found to decrease for the degraded sample compared to the non-degraded one. The reason for this is probably swelling of the polymer film upon ingression of water. Due to structural degradation, the exposed sample now allows large amounts of water to enter the polymer matrix and reach the polymer-ZnSe interface. Hence, there is a significant decrease in the density of the macromolecular structure within the probing depth of the evanescent field. As this was not or hardly observed for the unexposed sample, the effect has to be attributed to structural changes of the polymer after exposure to ozone, humid air and UV-B radiation.

To understand the kinetics of water uptake through both the samples after the first spectrum was collected within 2 minutes of exposure, ATR-FTIR spectra were collected every 5 minutes for 2 hours. Figure 3.5 shows the ATR-FTIR spectra of the degraded PVB sample upon exposure to de-ionized water taken every 5 minutes over a period of 2 hours. The ATR-FTIR spectrum of the PVB collected within 2 minutes of exposure to liquid water was used as the background. Hence, the observed changes are only due to ingression of water in the film and there are no polymer bands visible. From the spectra, it can be seen that the degraded polymer gets saturated with water within the first 20 minutes of exposure. To understand better, the absorbance at 3450 cm^{-1} is plotted as a function of exposure time in Figure 3.6. As can be seen, the absorbance shows an abrupt increase from 0.1009 to 0.119 and remains almost constant (0.12) over the remaining exposure period. For the unexposed sample (Figure 3.7), the water uptake is much more gradual compared to the degraded PVB film. Here also, the ATR-FTIR spectrum of the intact polymer collected within 2 minutes of exposure to liquid water was used as the background. The absorbance values were found to increase slowly but steadily from approximately 0.026 to 0.0641 over the span of 2 hours as shown in Figure 3.8 but the polymer was not saturated in the investigated time bracket. This indicates that there has been deterioration in the water resistive properties of the film after exposure to ozone, humidity and UV-B radiation in a way that the PVB-ZnSe interface gets saturated within 20 minutes of exposure. Also, the absorbance values are almost 4 times higher for the degraded sample, again due to a greater water uptake compared to the intact polymer. Exposure to ozone, humidity and UV-B radiation may have led to the formation of

numerous cracks and pores in the polymer matrix leading to enhanced ingress of water though them to the PVB-ZnSe interface.

3.3 EXPOSURE TO UV AND MOISTURE

To verify if ozone is responsible for the structural changes in the PVB film, a PVB film spin coated on ZnSe was then exposed to 90% RH and UV-B only. Figure 3.9 shows the corresponding ATR-FTIR spectra before and after exposure. The pure ZnSe crystal was used as the background for both spectra. First, only a slight increase in O-H stretch intensity is observed which is due to water transport to the PVB-ZnSe interface. The presence of water is also evident from an increase in the 1645 cm^{-1} peak intensity, which is attributed to the water O-H deformation mode. To understand this better, the spectra have been zoomed in the 1500-1800 cm^{-1} region as shown in the inset of Figure 3.10. It is interesting to note that the increase in the O-H stretch band is almost negligible and much smaller than that observed when PVB was exposed to ozone, humidity and UV-B radiation. This indicates that for the sample exposed to all the three agents, the increase in the O-H stretch peak was not contributed by the external water alone. In that case, the sample exposed to moisture and UV-B should have shown a similar change in the O-H stretch intensity. This however supports the fact that water is indeed generated as a degradation product when the sample is exposed to all the three agents and hence, accounts for the observed difference in the intensities of the OH band for the samples exposed to different sets of parameters.

Second, there was no change in the C=O stretch intensity at 1735 cm^{-1} as seen from the inset of Figure 3.10. Again, the observed fine structure is due to the rotational transitions of the gaseous water molecules excited by the IR energy. It is important to recall that nitrogen gas is used to generate the humid air and there was no source of oxygen (atomic or molecular) for this exposure. So, this proves that an oxygen (atomic or molecular) source is required to bring about structural degradation of PVB.

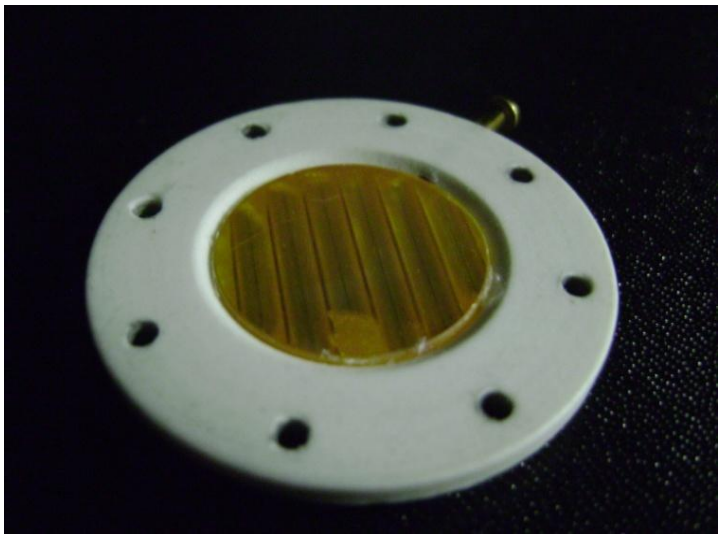

a

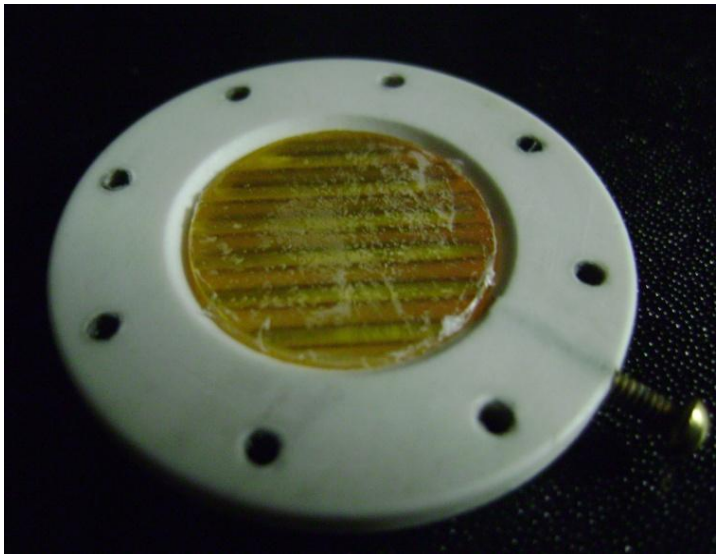

b

Figure 3.1a.PVB film on a ZnSe IRE **before** exposure to 0.1 ppm ozone, 90% RH and UV-B light **b**.PVB film on a ZnSe IRE **after** exposure to 0.1 ppm ozone, 90% RH (nitrogen) and UV-B light for 72 hours.

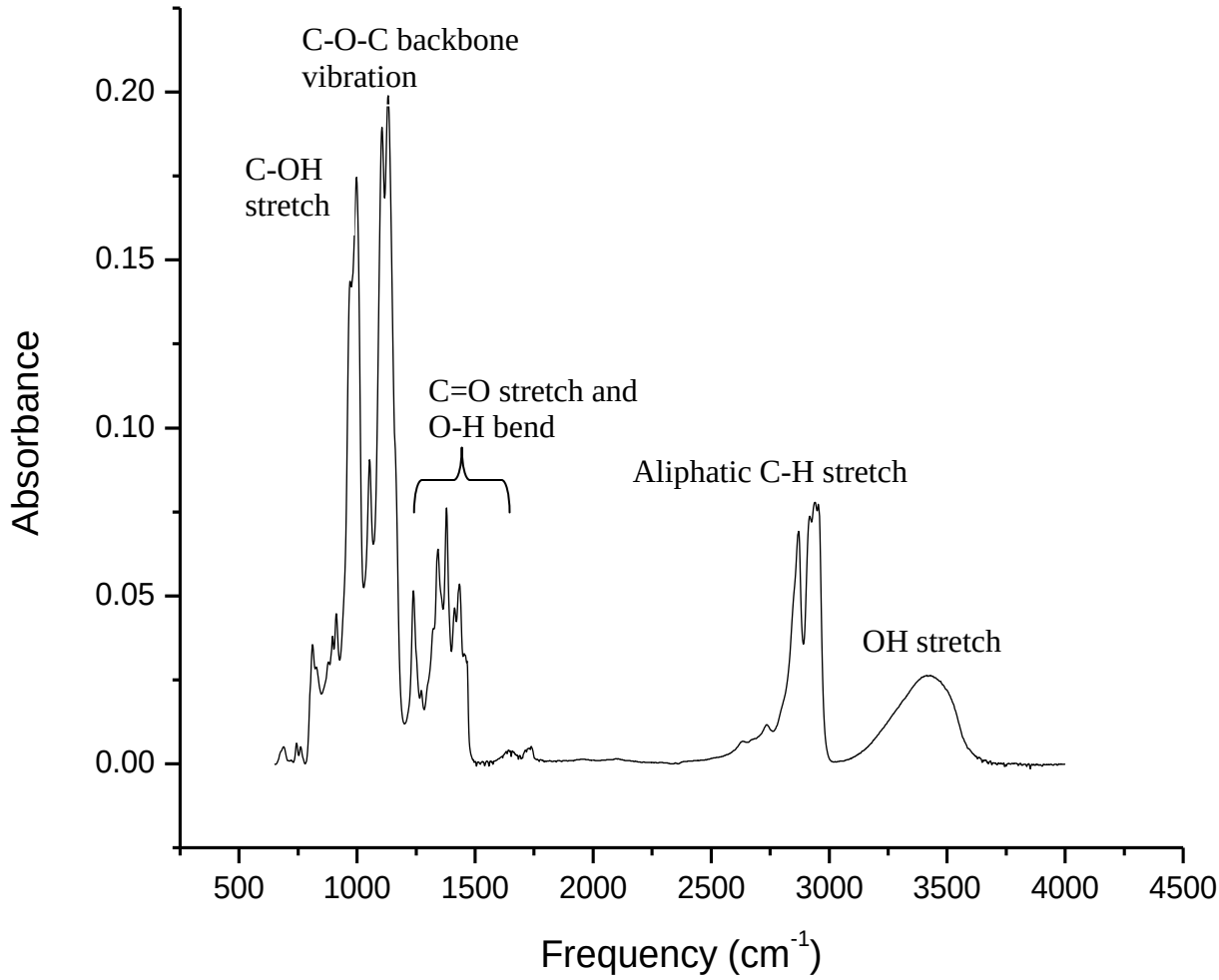

Figure 3.2.ATR-FTIR spectra of PVB spin coated on a ZnSe IRE. The pure ZnSe IRE was used as the background. The spectrum is averaged over 400 scans.

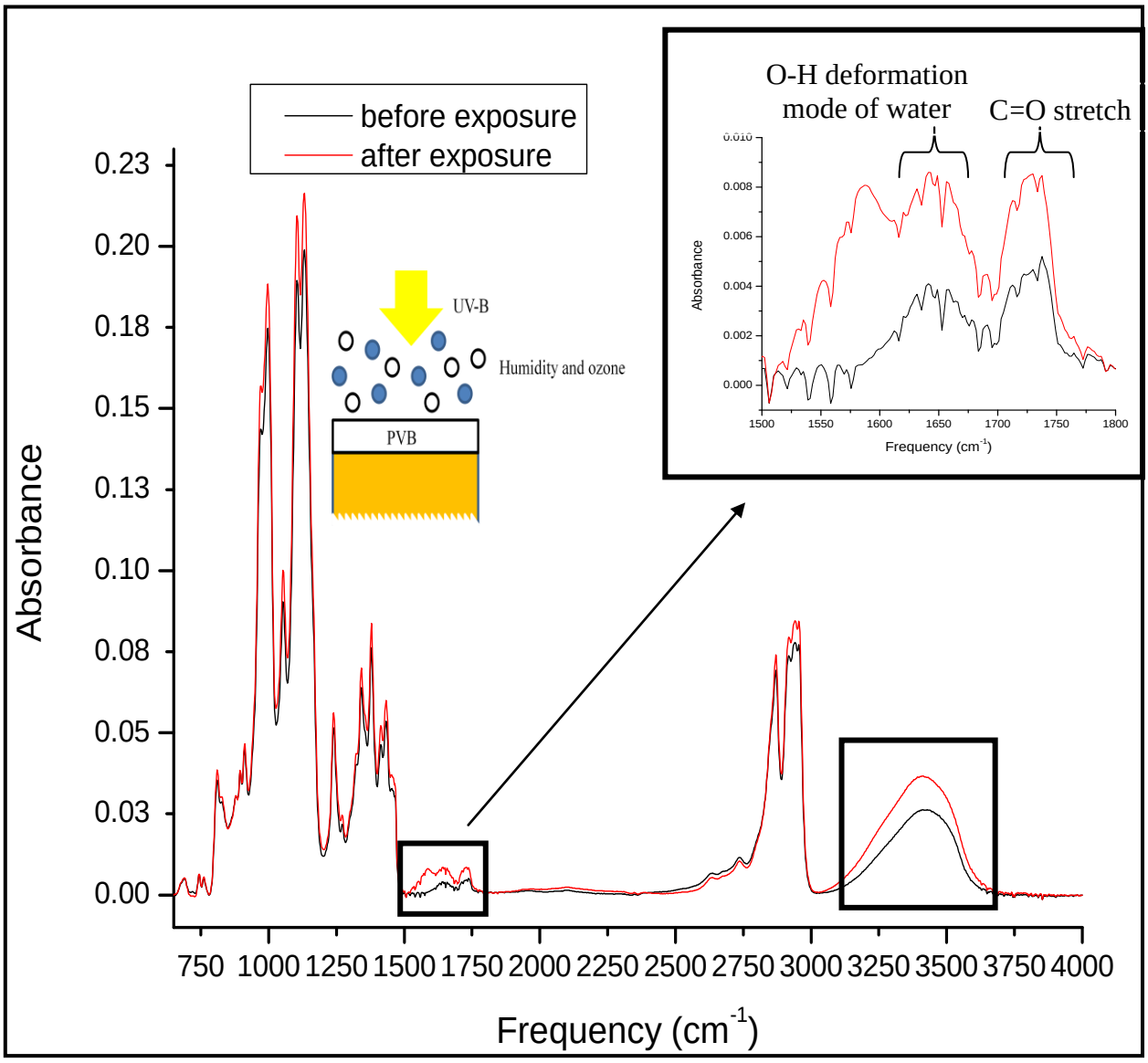

Figure 3.3.ATR-FTIR spectra of PVB spin coated on a ZnSe IRE before and after exposure to 0.1 ppm ozone, 90% RH and UV-B (310 nm) radiation for 72 hours. The pure ZnSe IRE was used as the background for both spectra. Each spectrum is averaged over 400 scans. The inset shows the same spectrum zoomed in the region 1500-1800 cm^{-1} to show the intensity increase in both C=O stretch and O-H deformation modes.

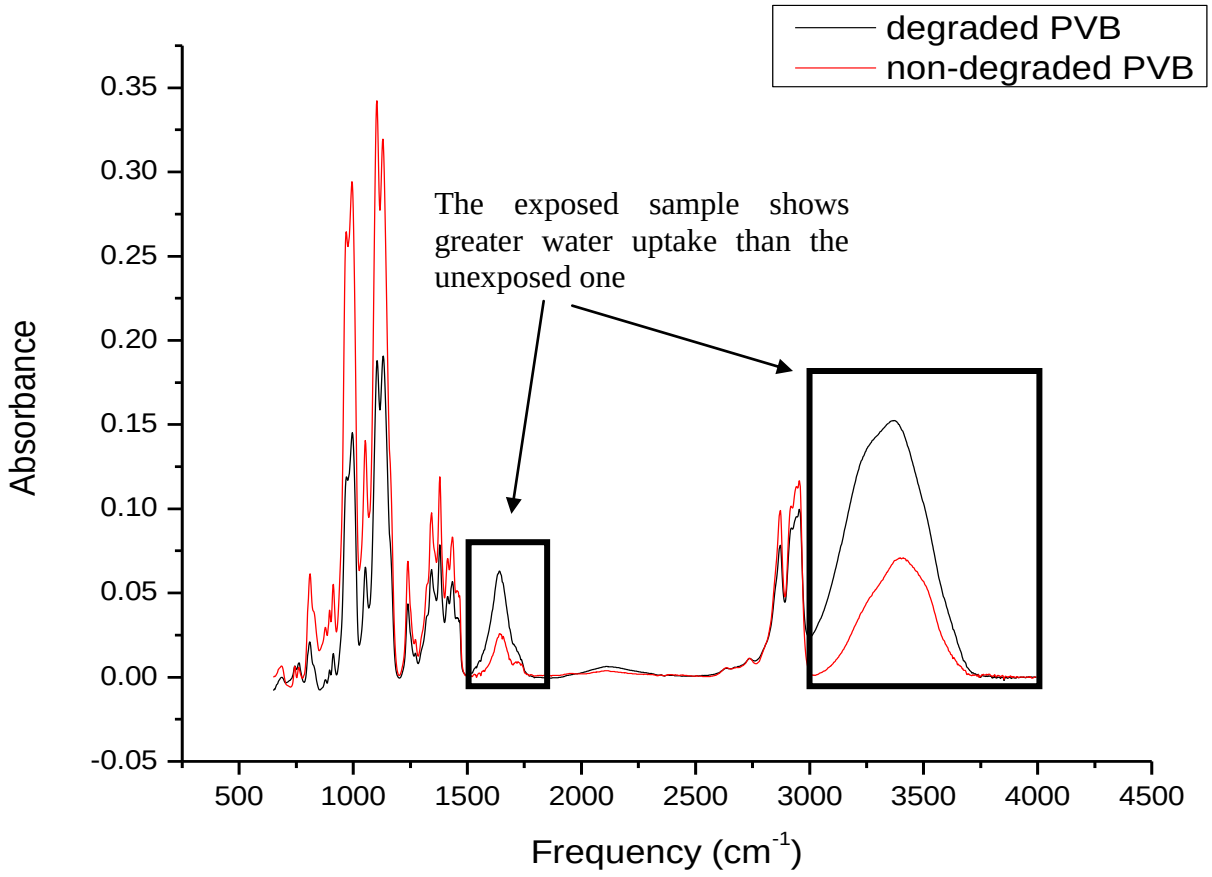

Figure 3.4.ATR-FTIR spectra of the degraded and non-degraded PVB samples in contact with de-ionized water within 5 minutes of exposure, using pure ZnSe as background and averaged over 128 scans.

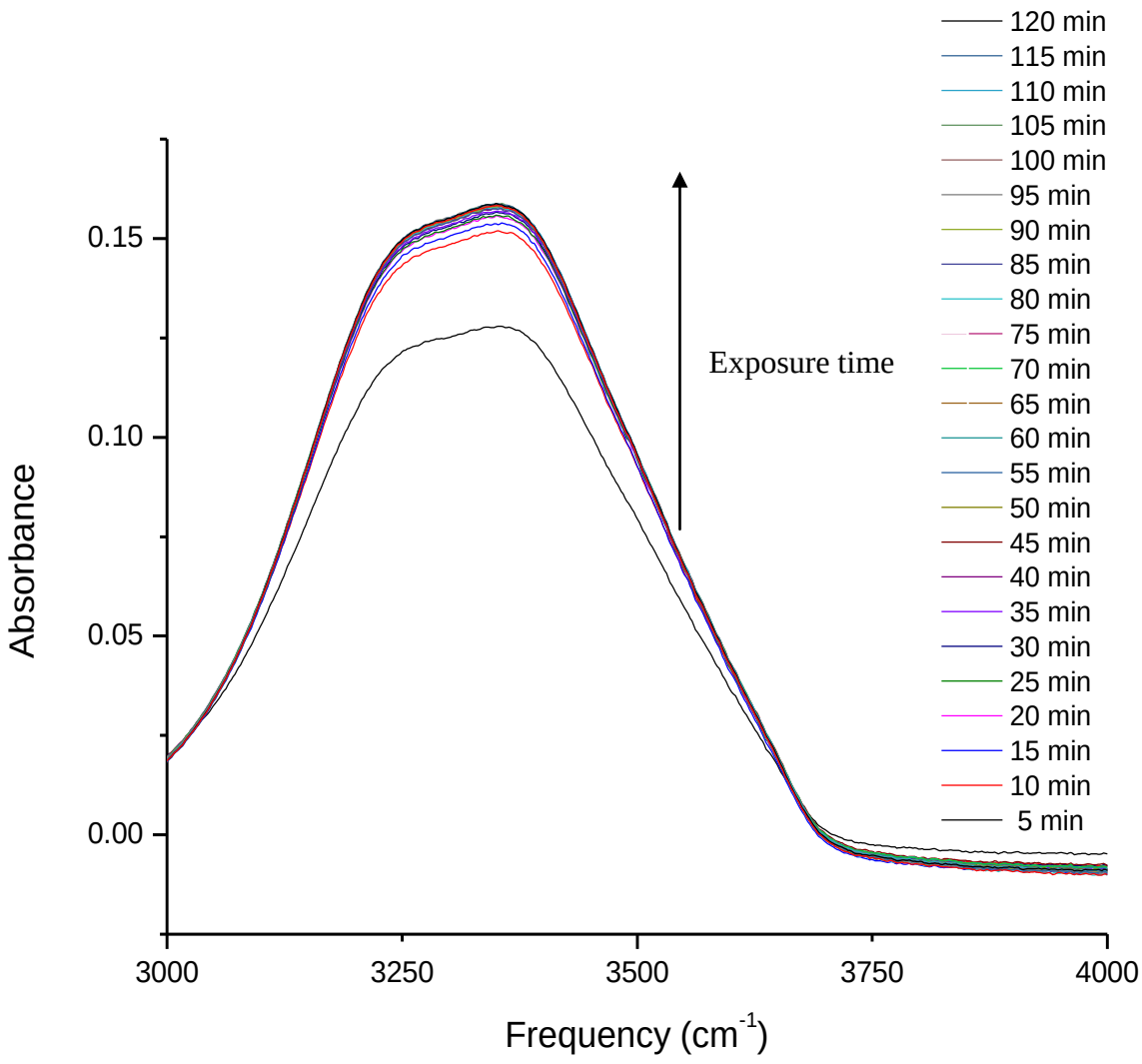

Figure 3.5.ATR-FTIR spectra of the **degraded** PVB sample showing abrupt water uptake upon exposure to de-ionized water over a period of 2 hours. The degraded polymer was used as the background after drying in a desiccator for 48 hours. Each spectrum is averaged over 128 scans.

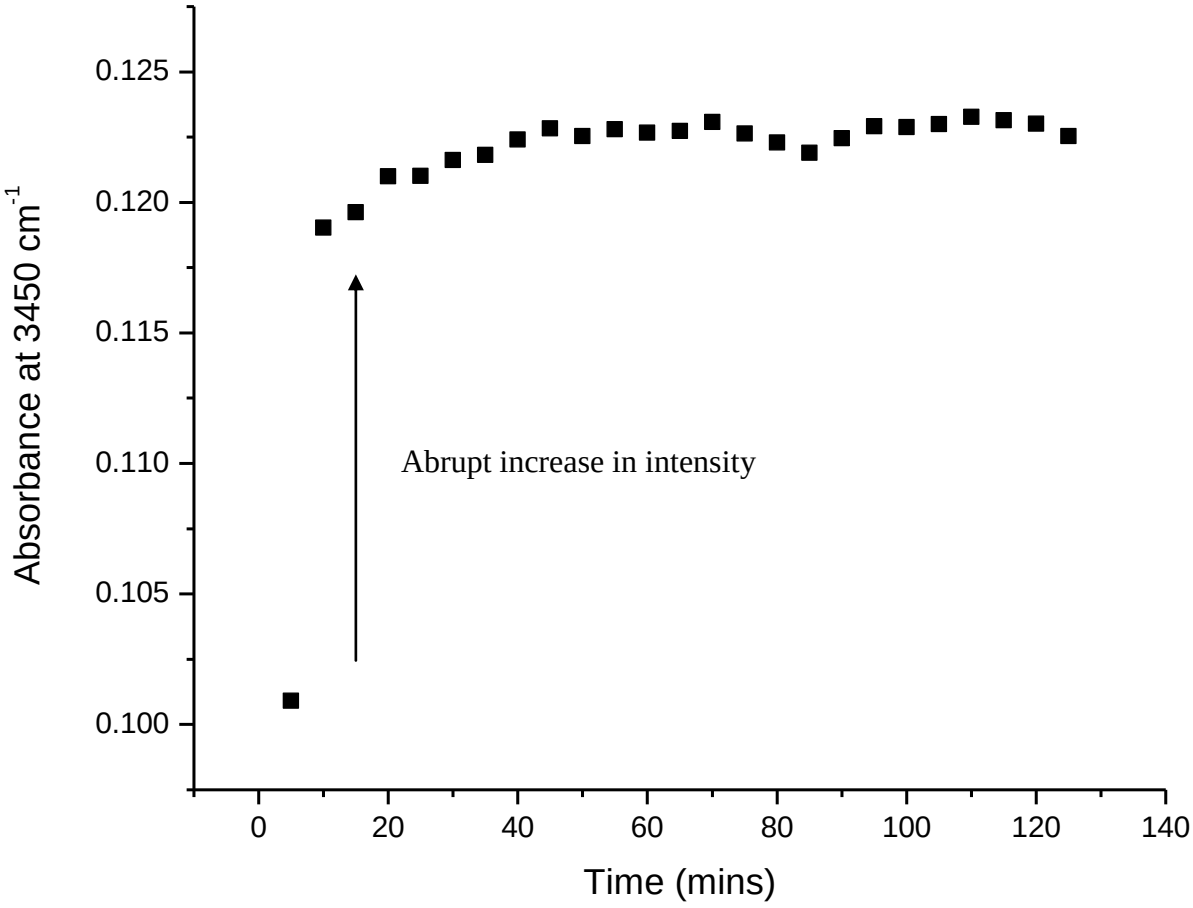

Figure 3.6.IR absorption intensities at 3450 cm^{-1} vs. exposure time for the **degraded** PVB film spin coated on a ZnSe IRE in contact with de-ionized water.

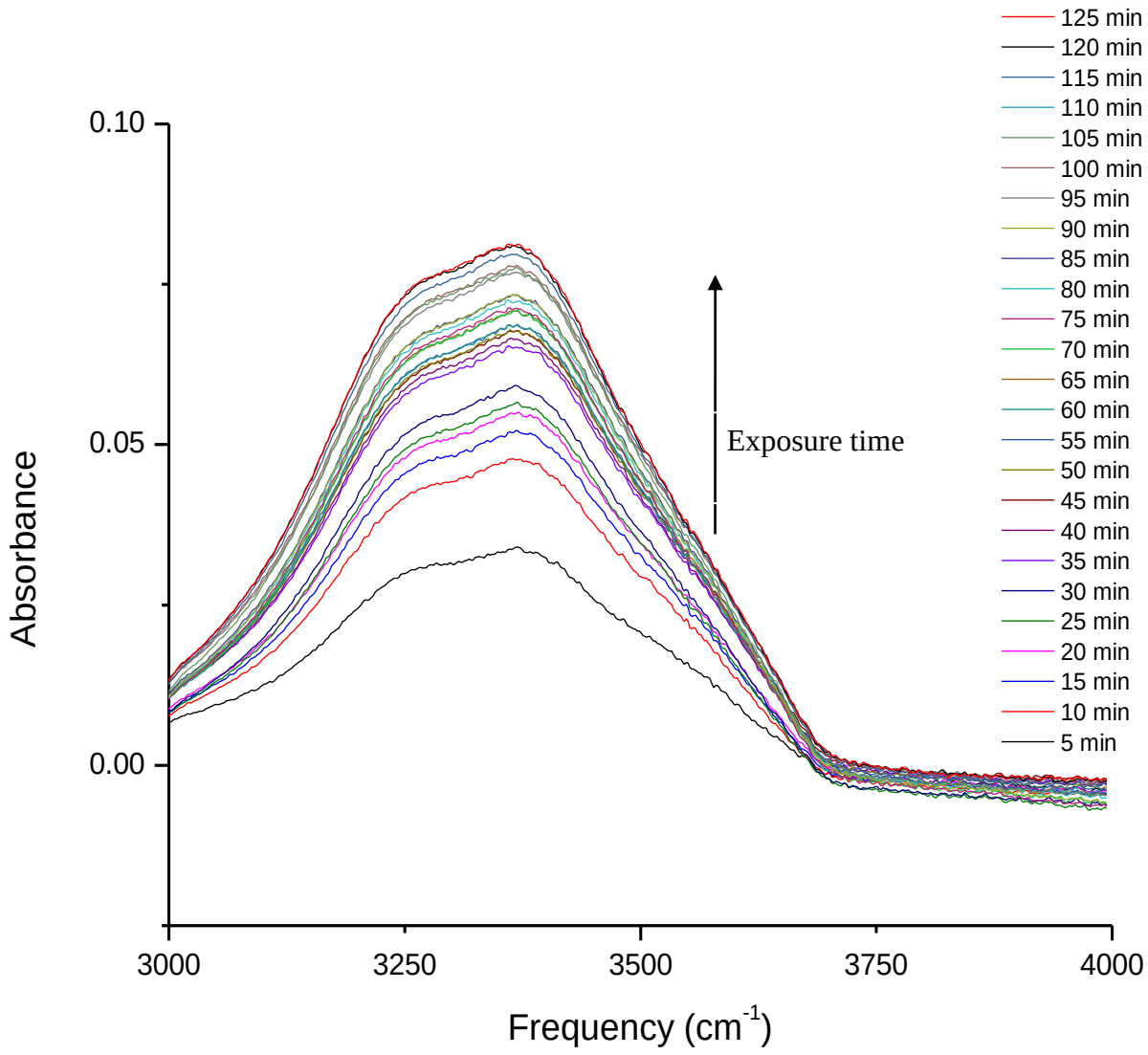

Figure 3.7.ATR-FTIR spectra of the **non-degraded** PVB sample showing gradual water uptake upon exposure to de-ionized water over a period of 2 hours. The dry polymer was used as the background. Each spectrum is averaged over 128 scans.

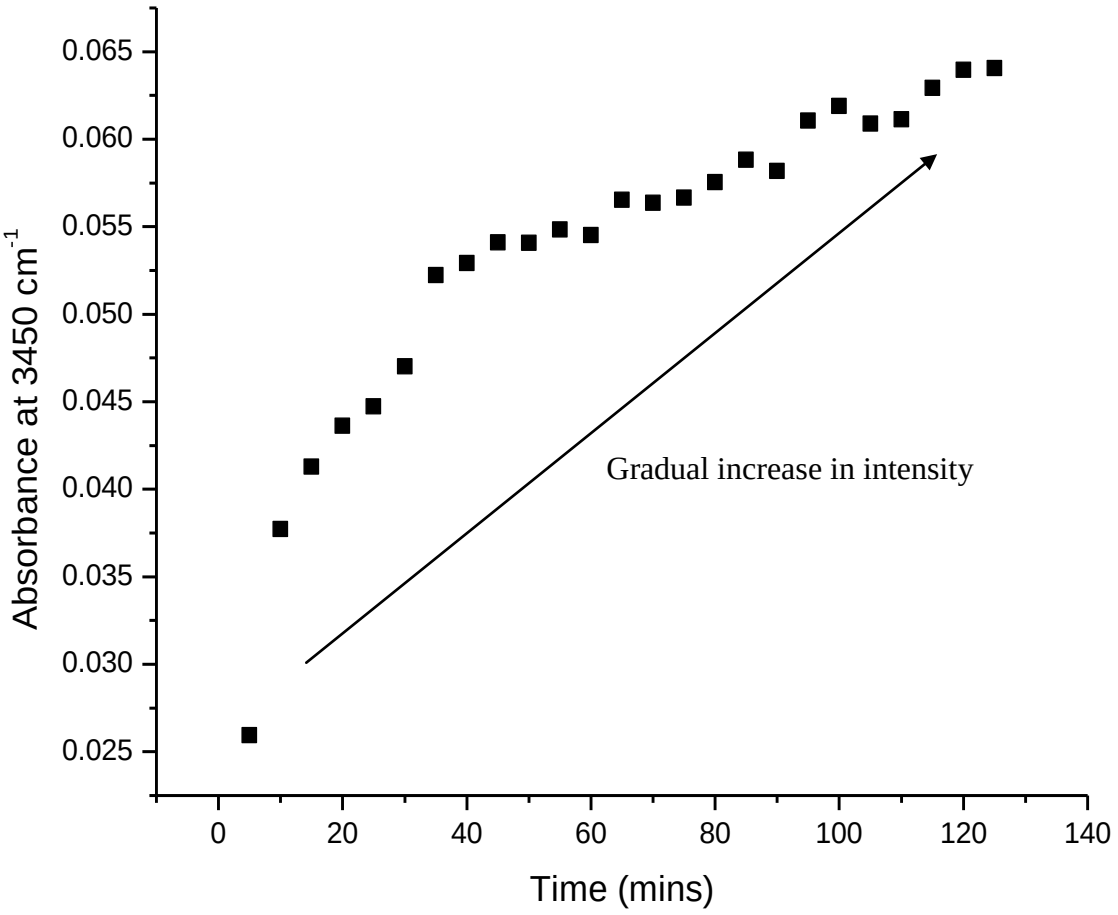

Figure 3.8.IR absorption intensities at 3450 cm^{-1} vs. exposure time for the **non-degraded** PVB film spin coated on a ZnSe IRE in contact with de-ionized water.

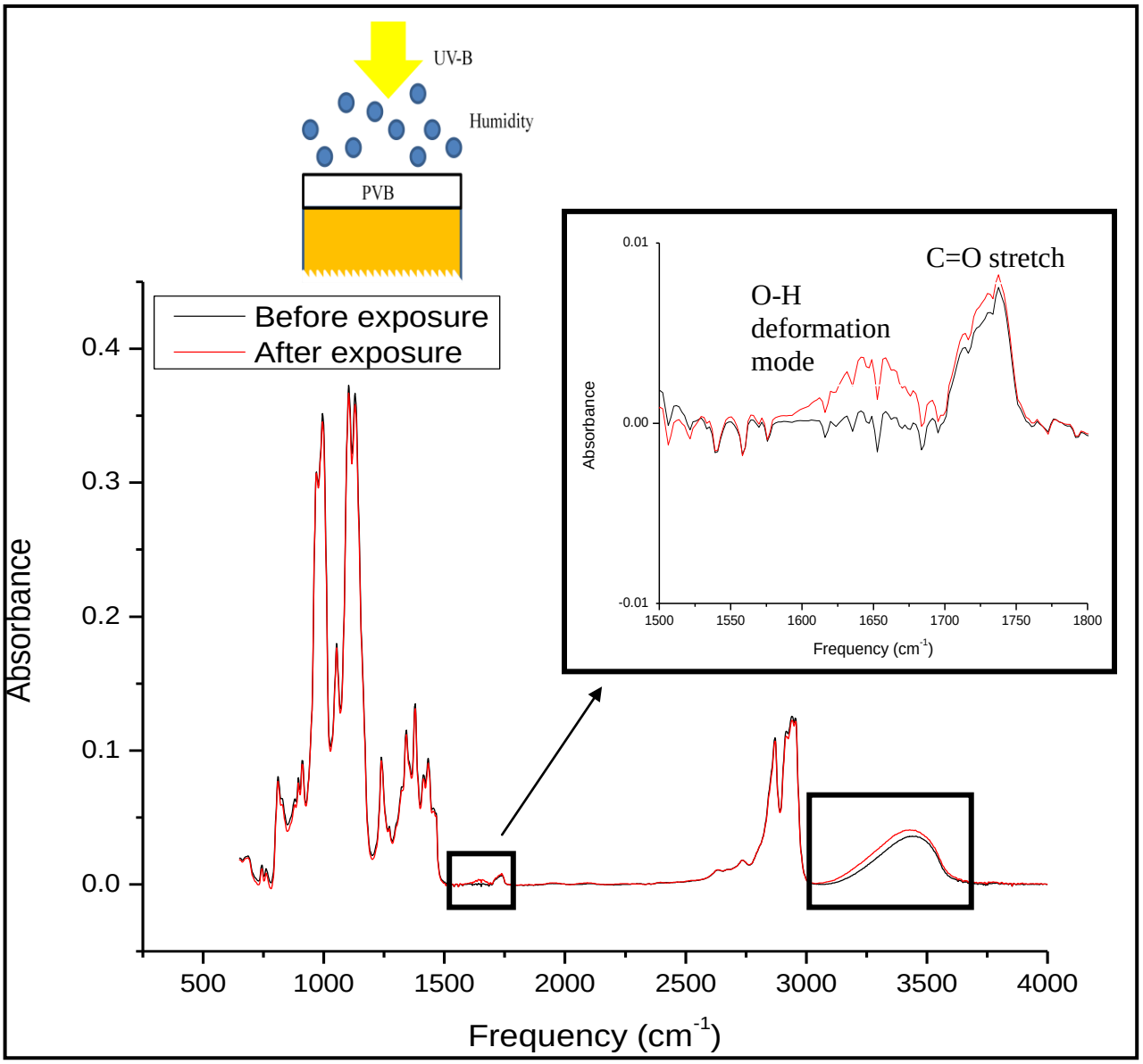

Figure 3.9.ATR-FTIR spectra of PVB spin coated on a ZnSe IRE before and after exposure to 90% RH and UV-B (310 nm) radiation for 72 hours. The pure ZnSe IRE was used as the background for both spectra. Each spectrum is averaged over 400 scans. The inset shows the same spectrum zoomed in the region 1500-1800 cm^{-1} to show the intensity increase in the O-H deformation mode only.

Chapter 4

RESULTS AND DISCUSSION: WATER UPTAKE BY POLYMER COATED ALUMINUM: STABILITY OF ALUMINUM-POLYMER INTERFACES

4.1 WATER UPTAKE BY PVB-COATED ALUMINUM

In this chapter the results on water transport to aluminum-PVB interfaces monitored using ATR-FTIR spectroscopy are discussed. They are compared to measurements with an aluminum-eponol system. To investigate the response of the Al-PVB interfacial zone to liquid water, samples as described above were exposed to de-ionized water as shown in Figure 4.1. Figure 4.2 shows the corresponding ATR-FTIR spectra at different exposure times. The background spectrum was collected from the dry sample before exposing it to the water and is represented by the horizontal line at zero absorbance. Hence the spectral features indicate only the changes occurring at the PVB-Al interface upon exposure to water. As can be seen from the spectra, a broad and strong band appeared between 3000 and 3700 cm^{-1}, with a maximum at around 3450 cm^{-1} and continued to grow as a function of exposure time. This peak is attributed primarily to both symmetric and asymmetric OH stretching vibrations of water molecules although there may be minimal contributions from OH stretching due to aluminum hydroxide

formation at the interface.[22,31] The increase in peak area indicates that the evanescent field generated at the PVB-Al interface encounters more and more water molecules within its reach with increase in exposure time and also possibly formation of aluminum hydroxide at the probed interface. It is known that water is capable of displacing the weaker polymer-metal interactions with stronger water-metal oxide/hydroxide bonds (40-65 kJ/mol) at the interface, the process being thermodynamically favored.[40] The band at 1650 cm^{-1} can be assigned to the deformation mode of water molecules while those at and below 1100 cm^{-1} are attributed to contributions from other water modes and Al corrosion products. It is known that various Al-O and Al-OH modes appear in the region 850 – 1100 cm^{-1}.[60] These can be a mixture of OH bending vibrations and twisting of AlOOH and also, Al-O vibrations of Al_2O_3.[31] With increase in exposure times, a small but sharp peak appeared at about 980-1000 cm^{-1}. The inset in Figure 4.2 shows that this peak actually grows with time and is assigned to the longitudinal stretching vibrations of Al-O[22] indicating that ingress of water at the PVB-Al interface corrodes the Al thin film beneath the PVB layer. This peak is also observed when a 50 nm Al film (without PVB) is exposed to de-ionized water for 5 hours, as shown in Figure 4.3. The Al film before exposure was used as the background. Other Al-O/Al-OH modes are also visible in the 850-1200 cm^{-1} region in addition to the obvious water peaks at 3400 and 1640 cm^{-1}. The negative peak at around 2350 cm-1 is due to a decrease in carbon dioxide within the probing depth of the evanescent field upon exposure to water.

The OH stretch band (3000-3700 cm^{-1}) shape is highly indicative of the physical state of water incorporated at the PVB-Al interface. It is well known that water confined in a hydrophilic polymer behaves differently than water in bulk liquid phase due to interactions of water molecules with the polar groups of the polymer leading to their restricted motion, either directly or through other water molecules.[61] Water has been found to exist in the form of clusters, chains and dimers etc. in hydrophilic polymers.[53] Water might also be incorporated in the porous oxide/hydroxide film at the interface. To understand how this compares with pure water structure, the ATR-FTIR spectrum of de-ionized water (OH stretch region) along with its calculated fit including the component peaks is depicted in Figure 4.4. The overall spectrum could be fitted using three Gaussian peaks. In accordance with the generally accepted assignments.[62] the component peak at about 3200 cm^{-1} can be attributed to the strong intermolecular coupling of water molecule symmetric stretch modes within a symmetric hydrogen bonding environment. The peak at about 3400 cm^{-1} is due to the weaker interactions of water stretching vibrations associated with a more distorted hydrogen bonding network. The peak at about 3510 cm^{-1} is assigned to the coupling of the asymmetric stretching vibrations of the water molecules. The fitting result for water incorporated at the PVB-Al interface is shown in Figure 4.5. Similar to pure water, water trapped at the PVB-Al interface can also be fitted using the three Gaussian peaks described above. Tables 4.1 and 4.2 give the fitting parameters for pure water and water in the PVB film respectively. As can be seen from the difference in band shape of the two spectra, there is an increased contribution from

the weakly hydrogen bonded water molecules (peak at 3400 cm^{-1}) relative to the strongly bonded ones (3200 cm^{-1}) in the polymer than in pure water. Such an observation can be attributed to the breaking of the water network upon entering the polymer matrix and the weaker hydrogen bonding of water molecules to the polymer functional groups (polar sites), although the details of the electronic perturbation of the water molecules due to PVB is difficult to infer with this information.[63]

To understand the changes in the C-H stretching region (2800–3000 cm^{-1}) in more detail, the 5 hours exposed sample was plotted using the one hour exposed sample as the background as shown in Figure 4.6. Negative peaks in the region 2850 – 2960 cm^{-1} indicate that there is a decrease in C-H intensities with longer exposure to water. There can be two plausible explanations for such an observation. First, water incorporation in the polymer matrix may lead to swelling of the resin with the effect that the macromolecular structure of the polymer would be less dense within the probing depth of the evanescent wave. Second, the water reaching the interface will result in hydrolysis in wet de-adhesion processes. The polymer will partly de-adhere from the substrate and in that case, the absorption bands would be negative with respect to the intact interface.[22,27,40] However, it is not possible to distinguish between swelling and delamination using ATR-FTIR data. Delamination and swelling effects are even more prominent when a ZnSe IRE spin coated with a 10 μm PVB film only is exposed to de-ionized water. Figure 4.7 shows the ATR-FTIR spectra of a ZnSe IRE spin coated with a 10 μm PVB film only exposed to de-ionized water with the pure ZnSe as background. The C-H region has been zoomed in the inset of Figure 4.7.

4.2 WATER RETENTION AT THE PVB-ALUMINUM INTERFACE

After the water exposure experiments were concluded, both the PVB and Al-PVB samples were stored in an evacuated desiccator for over 48 hours till they appeared visually dry. Then, ATR-FTIR spectra were collected using these dried samples to see if water could still be detected at the corresponding interfaces, as shown in Figure 4.8. The respective dry sample data before exposure were used as the background. While the PVB sample showed no trace of water, an appreciable OH stretch band was still observed for the PVB-Al sample. This means that although PVB lost most of the water absorbed during exposure reversibly, a significant amount of water was trapped at the PVB-Al interface. It indicates that the now hydrophilic Al surface seems to be responsible for such water retention. Extensive research on aluminum surfaces has revealed the complex nature of such surfaces.[64-66] On an aluminum surface, a thin layer of aluminum oxide is always spontaneously formed in contact with air.[30] It is known that native surface layers on Al are made up of an anhydrous inner layer of amorphous Al_2O_3 covered by a hydrated outer layer, the latter being extremely important for the adhesion properties of the metal.[67] α-Al_2O_3 (corundum) and γ-Al_2O_3 are known to be the common oxides of aluminum. The oxy-hydroxides include α-AlO(OH) (diaspore) and γ-AlO(OH) (boehmite) while bayerite, gibbsite and nordstrandite are the three forms of hydroxides formed. In contact with water, hydroxyl functionalities are incorporated into either octahedral or tetrahedral sites on the crystal structure of alumina.[30,64] The oxide layers

are generally considered to be non – crystalline and porous. Investigation on the nature of the oxide film on Al has revealed that the composition of the oxide ranges from anhydrous to trihydroxide, depending on the temperature and pressure at which it was formed. It is known that films grown in the range 20-90˚C exhibit a duplex structure consisting of an inner layer of a porous structure of pseudoboehmite (or poorly crystalline boehmite) and an outer layer of large bayerite crystals.[67] This is the temperature range relevant for the present study. It is known that boehmite is composed of layers of edge shared AlO_6 octahedra with terminal hydroxyl groups.[68] This oxide/hydroxide layer might differ morphologically when under a polymer layer but is still responsible for making the metal surface hydrophilic. Also, it is known that on a metal oxide/hydroxide surface, a water monolayer would spontaneously bond with the surface hydroxyl groups by replacing the weaker polymer-oxide/hydroxide linkages. Probably, such a surface structure is responsible for retaining water molecules at the interface by formation of hydrogen bonding as envisioned in Figure 4.9.

4.3 WATER UPTAKE BY EPONOL COATED ALUMINUM

It is interesting to compare the stability of the aluminum-PVB interface to water with that of a second polymer. Epoxy polymers are known to exhibit high adhesion and a good resistance to heat and chemicals. Hence, an epoxy polymer based on di-glycidyl ether of bisphenol A (DGEBA) was chosen for the purpose. It can be synthesized by reaction of bisphenol A and epichlorohydrin.[69] Different components in

the structure are known to perform specific functions to improve the resin's performance, for example, the polar –OH groups enhance adhesion with the substrate while the chain length determines the flexibility of the polymer.[70] Commercially, the resin comes in a blend of solvents, methyl ethyl ketone and propylene glycol methyl ether (75:25 wt %) and has the name eponol resin 53 BH 35.

Similar to the PVB-Al samples, an eponol coated aluminum-ZnSe sample was exposed to de-ionized water. The resulting changes of the eponol-Al interface structure were monitored with time. The corresponding ATR-FTIR spectra are shown in Figure 4.10. The dry sample before exposure was used as the background. The increase in intensity of the OH peak in the region 3000-3700 cm^{-1} indicates that more water was present at and near the aluminum-eponol interface because the penetration depth of the evanescent wave at the eponol-Al interface is smaller than that at the PVB-Al interface (Figures 2.2 and 2.3). This is further corroborated by an increase in the water OH deformation mode intensity at 1640 cm^{-1}. The peak at around 980-1010 cm^{-1}, attributed to the longitudinal Al-O modes was observed within the first hour of exposure but was found to remain almost constant over the remaining exposure period, in contrast to the aluminum-PVB system, where the peak was found to increase with time. The horizontal line at zero absorbance indicates the background i.e. the polymer coated aluminum before exposure to deionized water.

Similar to the aluminum-PVB system, fitting results of the water band (Figure 4.11) reveal that there is an increase in water molecules residing in a weakly hydrogen bonded environment relative to that seen in pure bulk water, where the dominant

contribution comes from associated (strongly hydrogen-bonded) chains of water molecules. The spectral fit parameters are given in Table 4.3.

Interestingly, both aliphatic and aromatic C-H peaks were found to increase in intensity relative to the dry sample with exposure time, again, in a striking contrast to what was observed at the PVB-Al interface when exposed to water. This increase is especially prominent after the sample was exposed to water for 15 hours. Figure 4.12 shows the corresponding ATR-FTIR spectrum. The dry sample before exposure was used as the background. Such an increase in C-H intensity was also observed when an eponol coated ZnSe sample (no aluminum) was exposed to 90% humidity for 20 hours. Figure 4.13 shows the corresponding ATR-FTIR spectrum. The dry polymer before exposure was used as the background. The reason for this observation is not fully understood but is probably related to a rearrangement of the macromolecular polymer chains within the matrix upon interaction with water molecules. It is clear that aluminum does not play a role in this C-H intensity increase. Although there isn't sufficient data to understand the processes going on when water interacts with eponol, it is clear that there are no swelling/delamination effects. On the basis of these observations, it can be inferred that eponol protects the aluminum film beneath itself better compared to PVB.

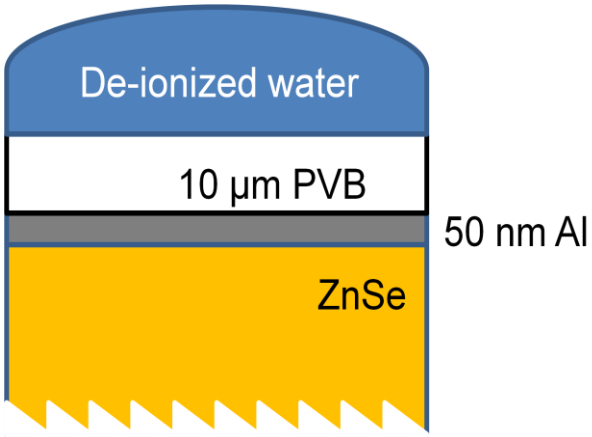

Figure 4.1.Schematic of an Al-PVB sample exposed to de-ionized water

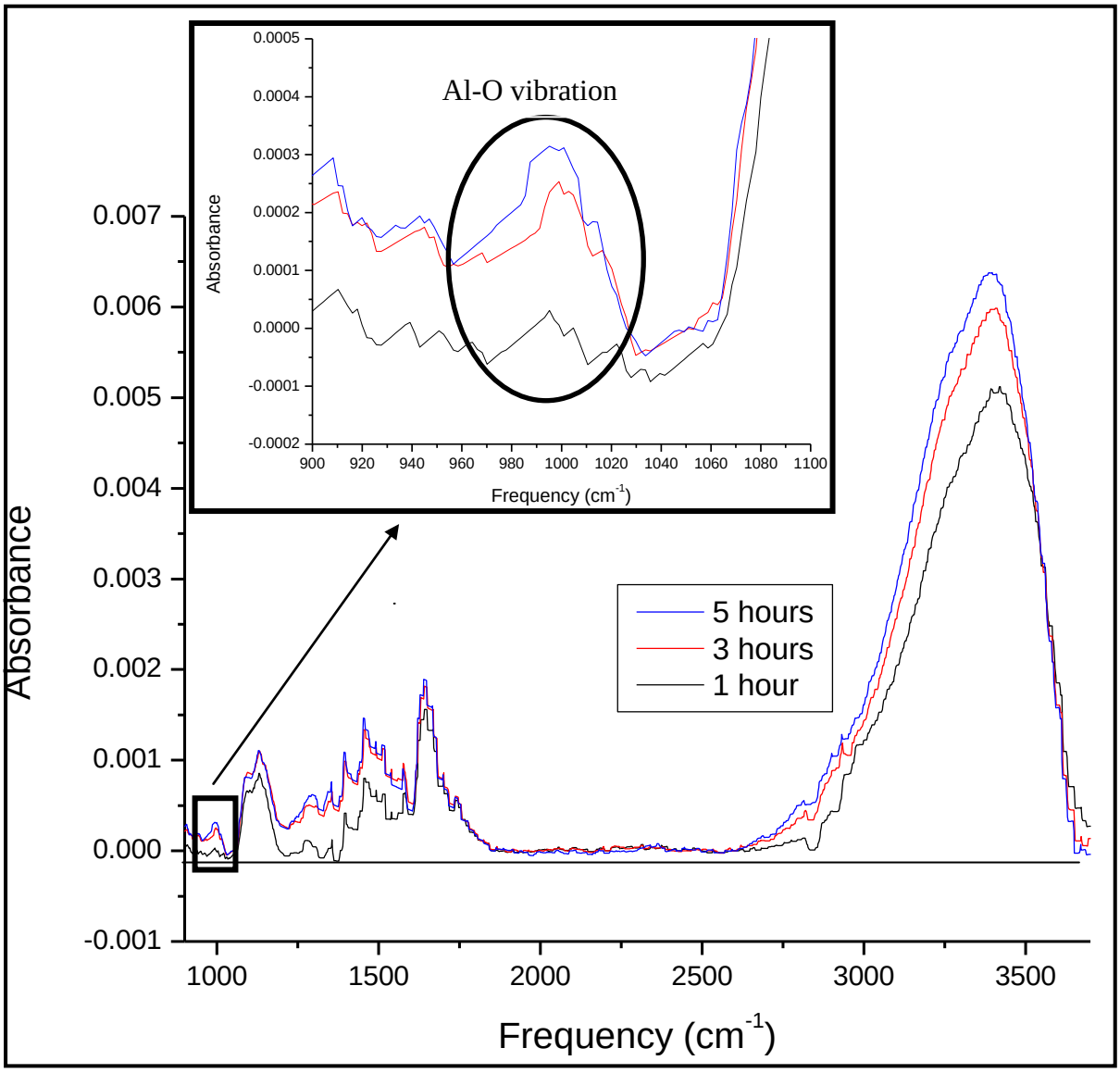

Figure 4.2.ATR-FTIR spectra of a ZnSe IRE sputter coated with a 50 nm Al film and a 10 μm PVB film in contact with de-ionized water with the dry sample before exposure as background. The exposure times were 1, 3 and 5 hours respectively. Each spectrum is averaged over 400 scans.

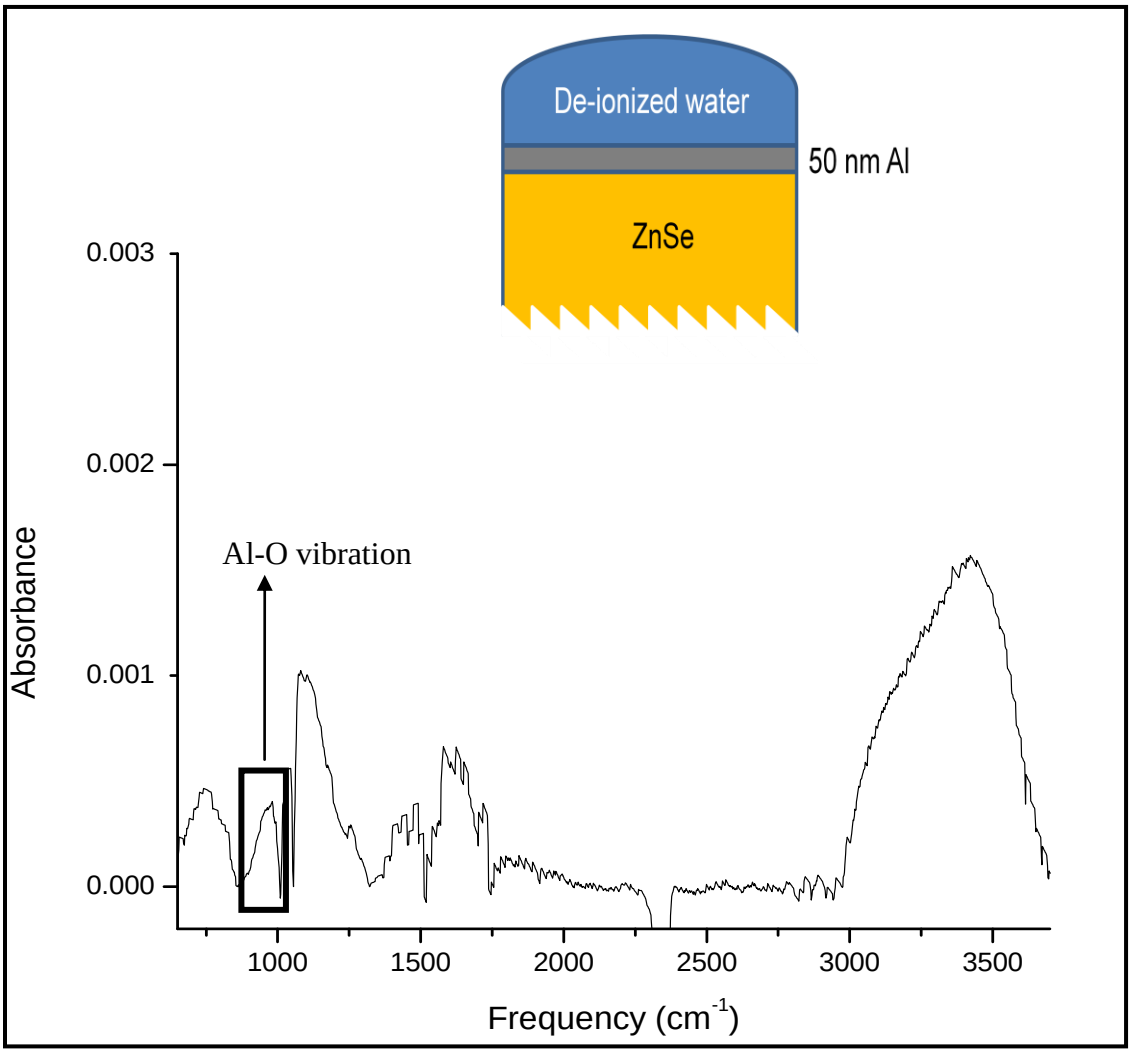

Figure 4.3.ATR-FTIR spectrum of a ZnSe IRE sputter coated with a 50 nm Al film in contact with de-ionized water for 5 hours with the dry sample before exposure as background and averaged over 400 scans.

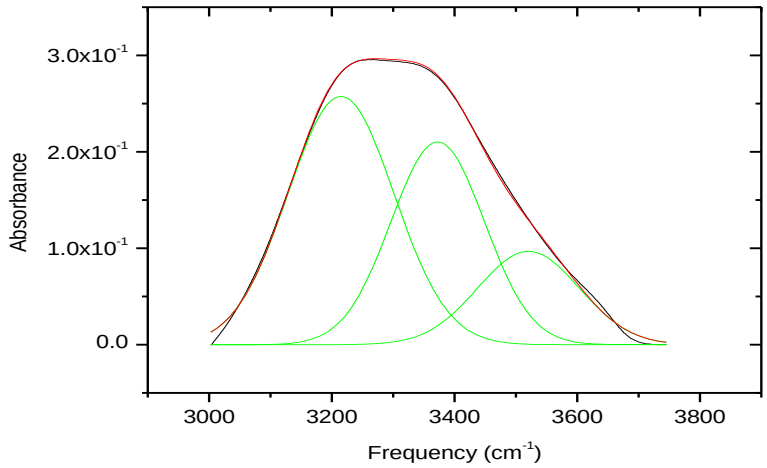

Figure 4.4. Peak fitting of the OH stretch mode of pure de-ionized water. 400 scans were acquired and the pure ZnSe was used as the background.

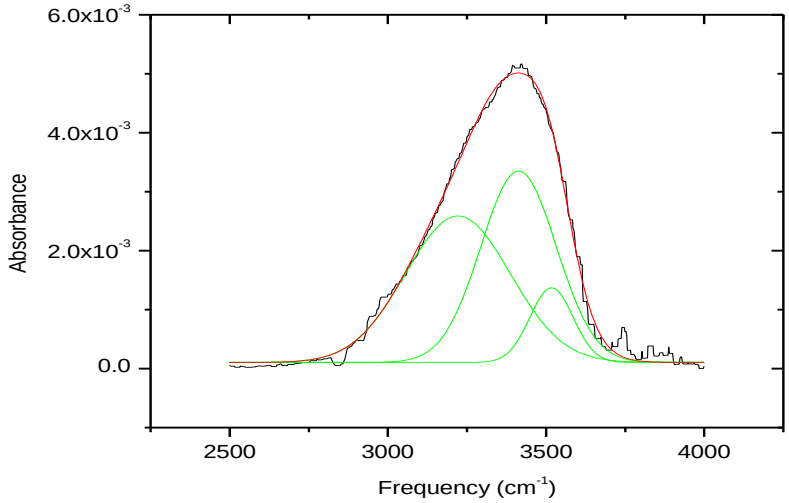

Figure 4.5. Peak fitting of the water OH stretch mode from the 1 hour water exposed aluminum-PVB sample.

Peak Index	Peak type	Area Integral	Peak center (cm^{-1})	Max. Height	FWHM (cm^{-1})
1	Gaussian	55.57428	3214.9	0.25735	204.36
2	Gaussian	40.1993	3372.5	0.21012	179.73
3	Gaussian	20.039	3520.5	0.09677	195.18

Table 4.1. Parameters for the pure water OH stretch spectral fits

Peak Index	Peak type	Area Integral	Peak center (cm^{-1})	Max. Height	FWHM (cm^{-1})
1	Gaussian	1.03023	3221.4	0.00248	389.78
2	Gaussian	0.97111	3413.1	0.00324	281.29
3	Gaussian	0.21646	3517.2	0.00126	160.79

Table 4.2. Parameters for PVB confined water OH spectral fits

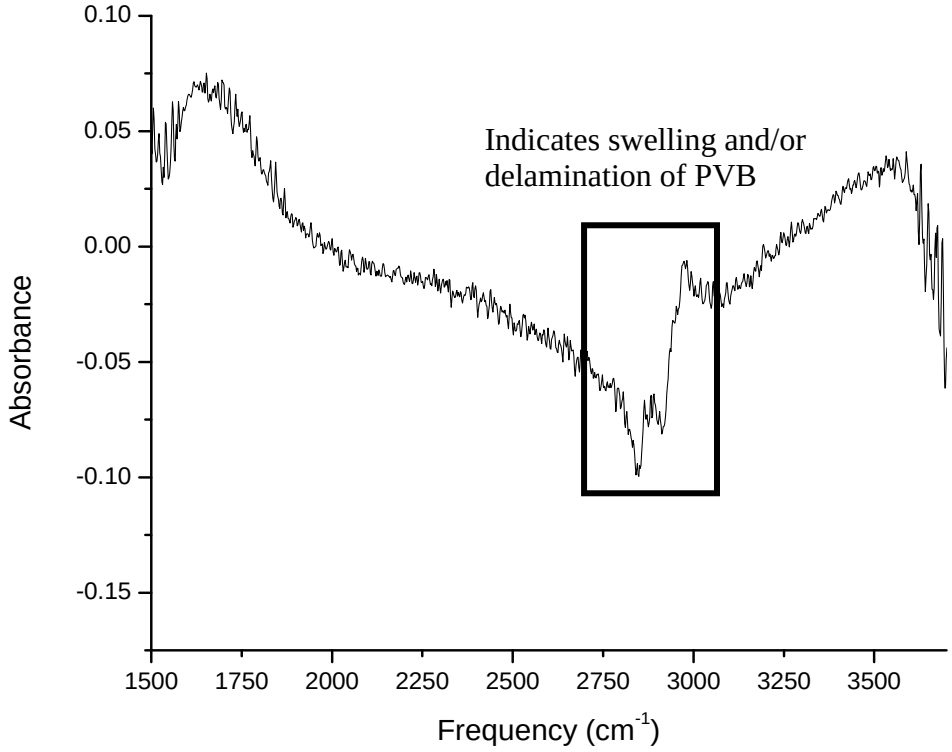

Figure 4.6.ATR-FTIR spectrum of A ZnSe IRE coated with 50 nm Al and PVB exposed to de-ionized water for 3 hours with the same sample exposed for 1 hour as the background. The spectrum is averaged over 400 scan.

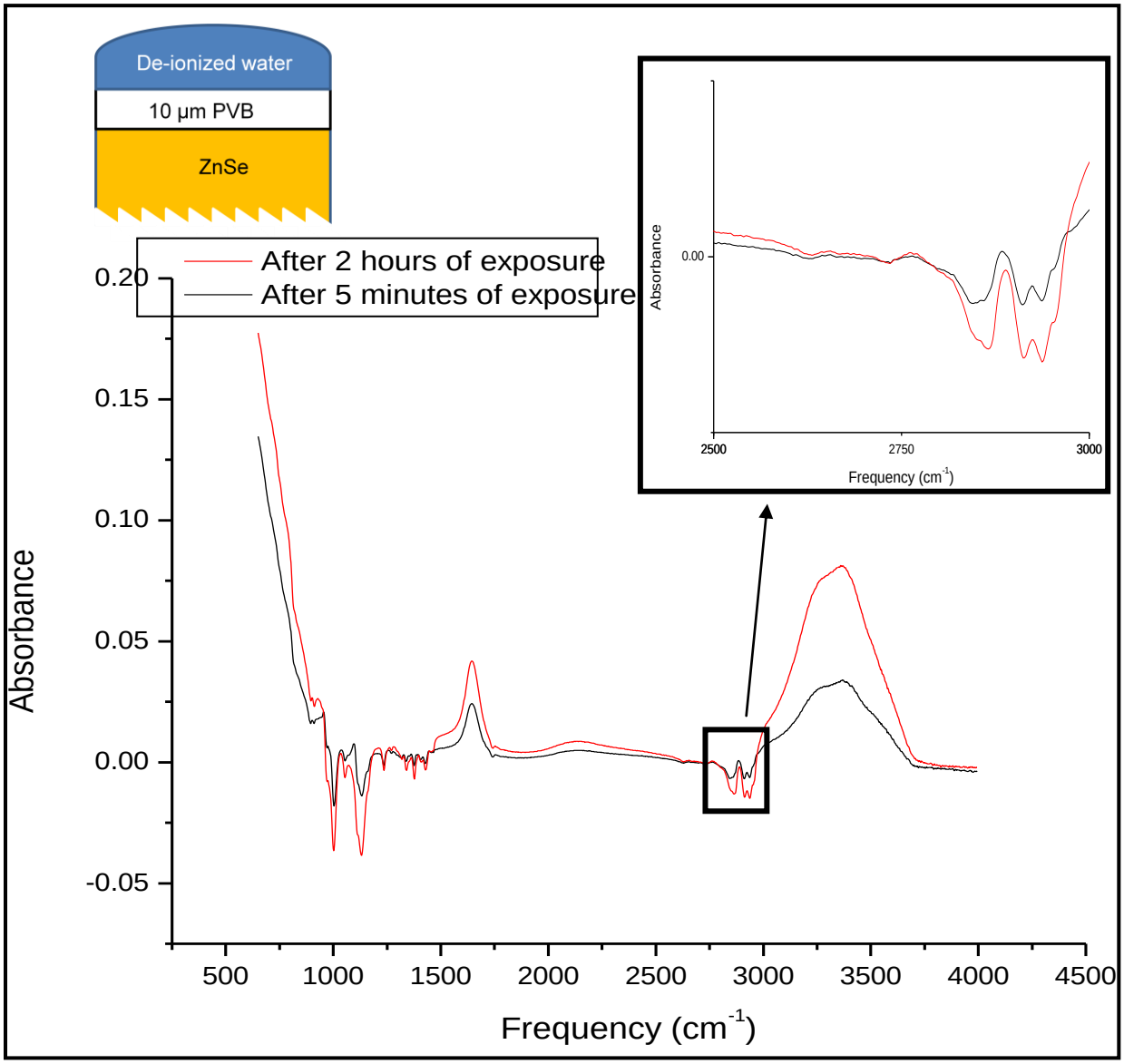

Figure 4.7.ATR-FTIR spectra of a ZnSe IRE spin coated with a 10 µm PVB film in contact with de-ionized water with the dry sample before exposure as background. The exposure times shown are 5 minutes and 2 hours. Each spectrum is averaged over 400 scans.

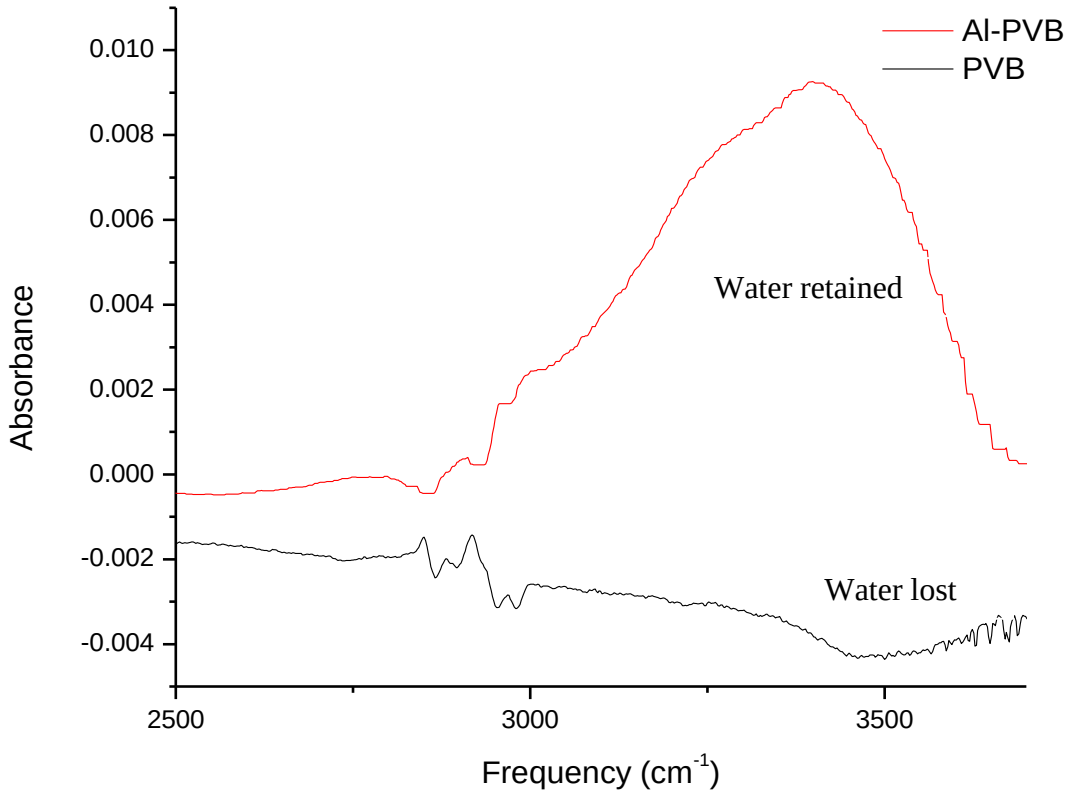

Figure 4.8.ATR-FTIR spectra of both Al-PVB and PVB samples dried over 48 hours after the water exposure experiments, using the respective dry samples (before exposure) as backgrounds. Each spectrum is averaged over 400 scans.

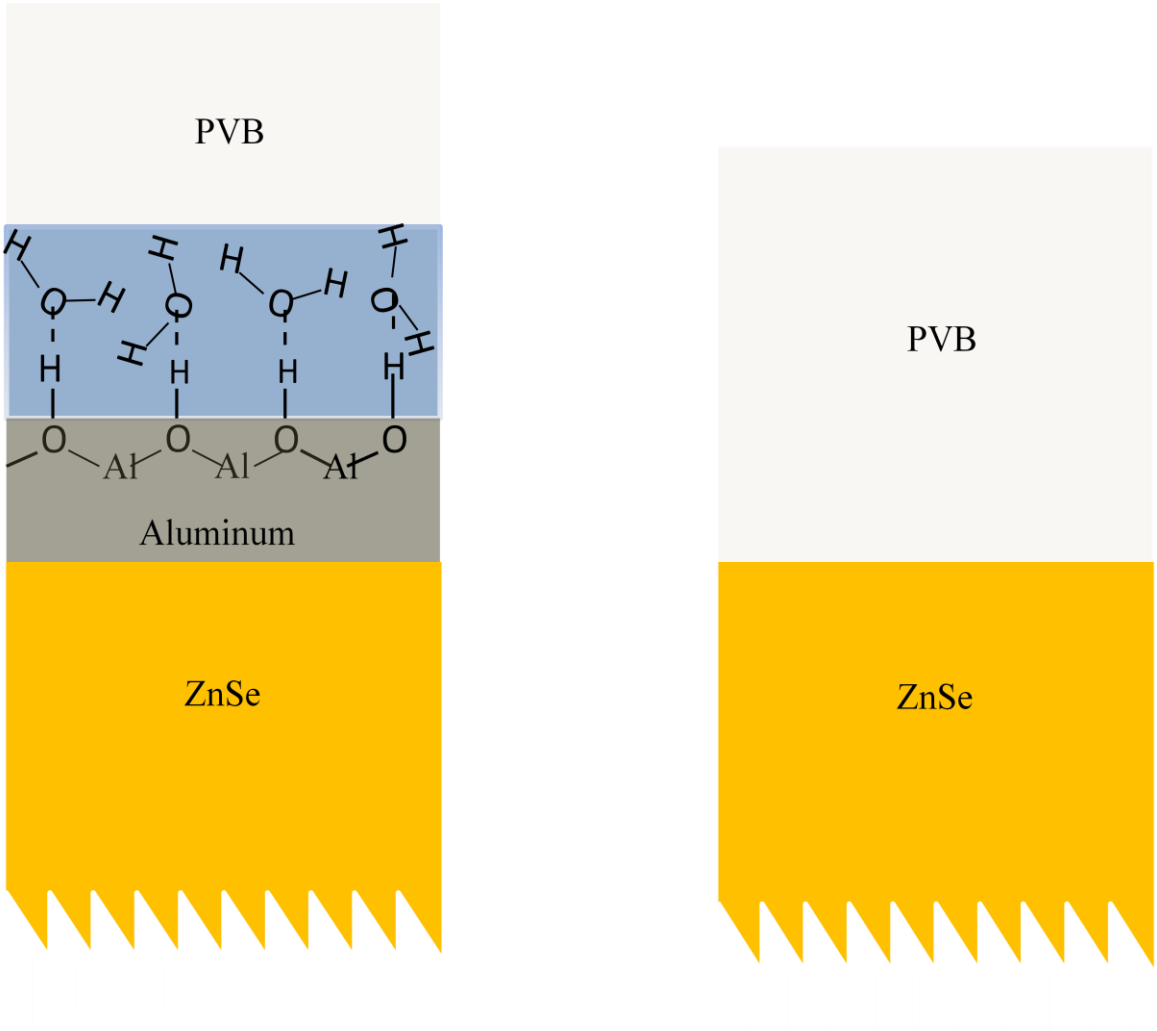

Figure 4.9. Schematic of the possible interactions of water molecules with the Al oxide/hydroxide film at the Al-PVB interface. PVB (right) loses water completely after drying.

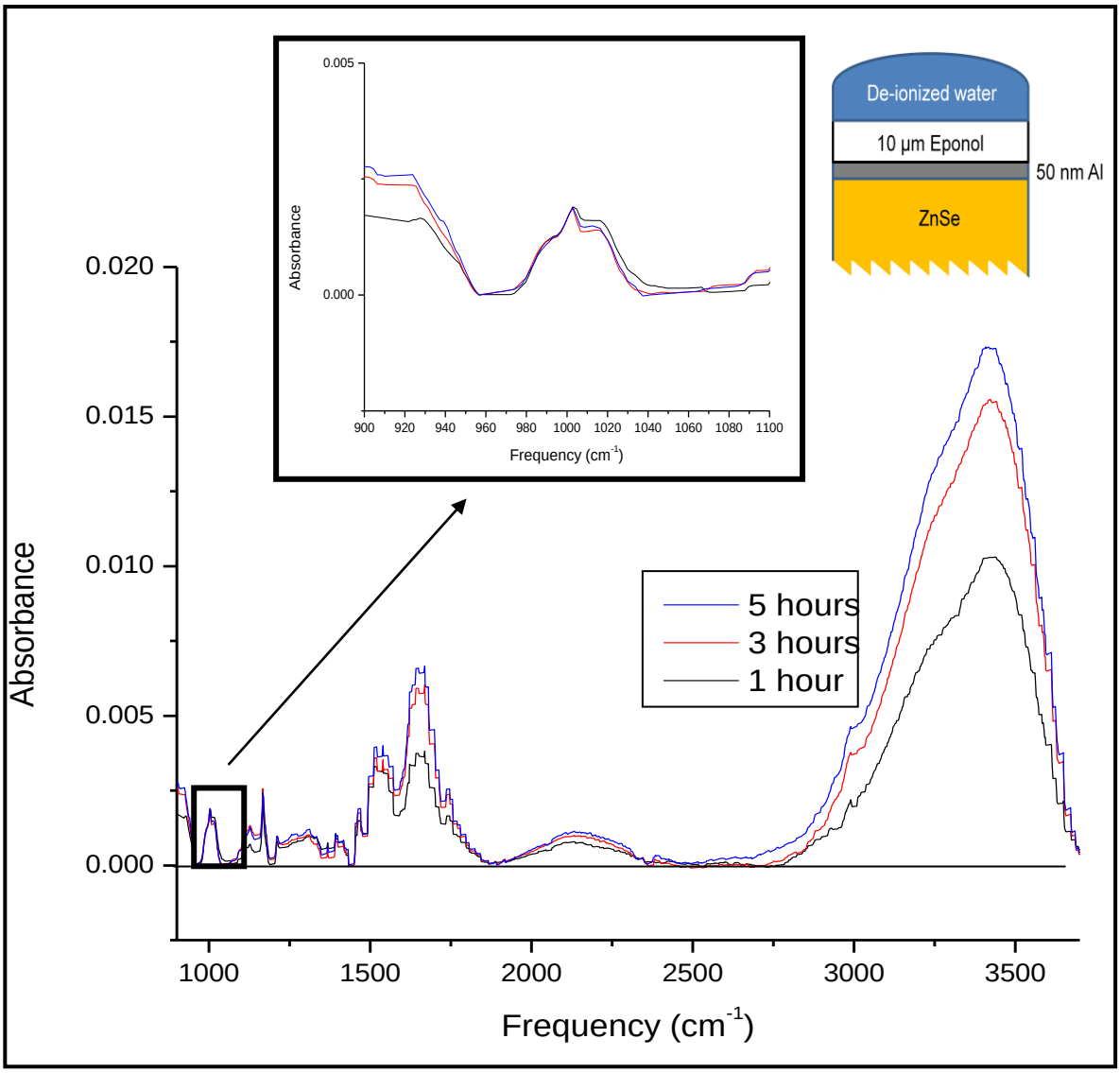

Figure 4.10.ATR-FTIR spectra of a ZnSe IRE sputter coated with a 50 nm Al film and a 10 µm eponol film in contact with de-ionized water with the dry sample before exposure as background. The exposure times were 1, 3 and 5 hours respectively. Each spectrum is averaged over 400 scans.

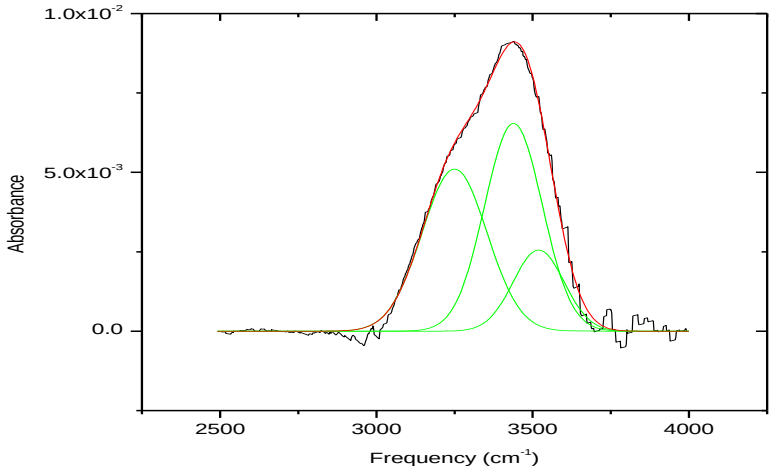

Figure 4.11. Peak fitting of the water band from the 1 hour exposed aluminum-eponol sample.

Peak Index	Peak type	Area Integral	Peak center (cm^{-1})	Max. Height	FWHM (cm^{-1})
1	Gaussian	1.33398	3250.1	0.0052	245.62
2	Gaussian	1.51372	3438.7	0.0065	217.46
3	Gaussian	0.52275	3519.1	0.0026	192.42

Table 4.3. Parameters for eponol confined water OH stretch spectral fits

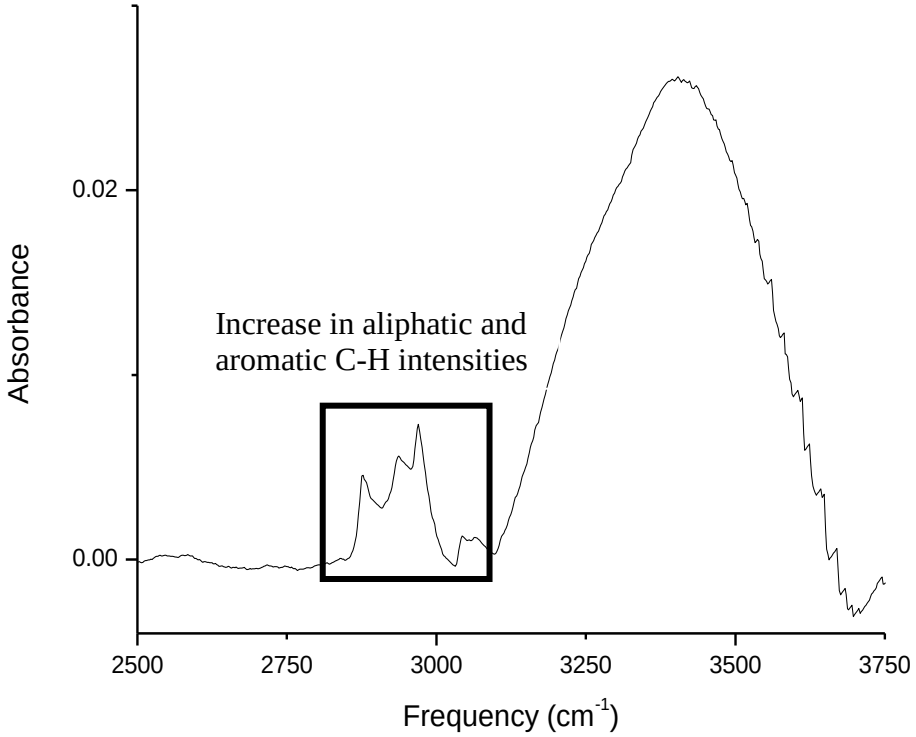

Figure 4.12.ATR-FTIR spectrum of a ZnSe IRE sputter coated with a 50 nm Al film and a 10 μm eponol film in contact with de-ionized water for 15 hours with the dry sample before exposure as background, zoomed in the region 2500 – 3700 cm^{-1} showing an increase in the C-H peak intensities and averaged over 400 scans.

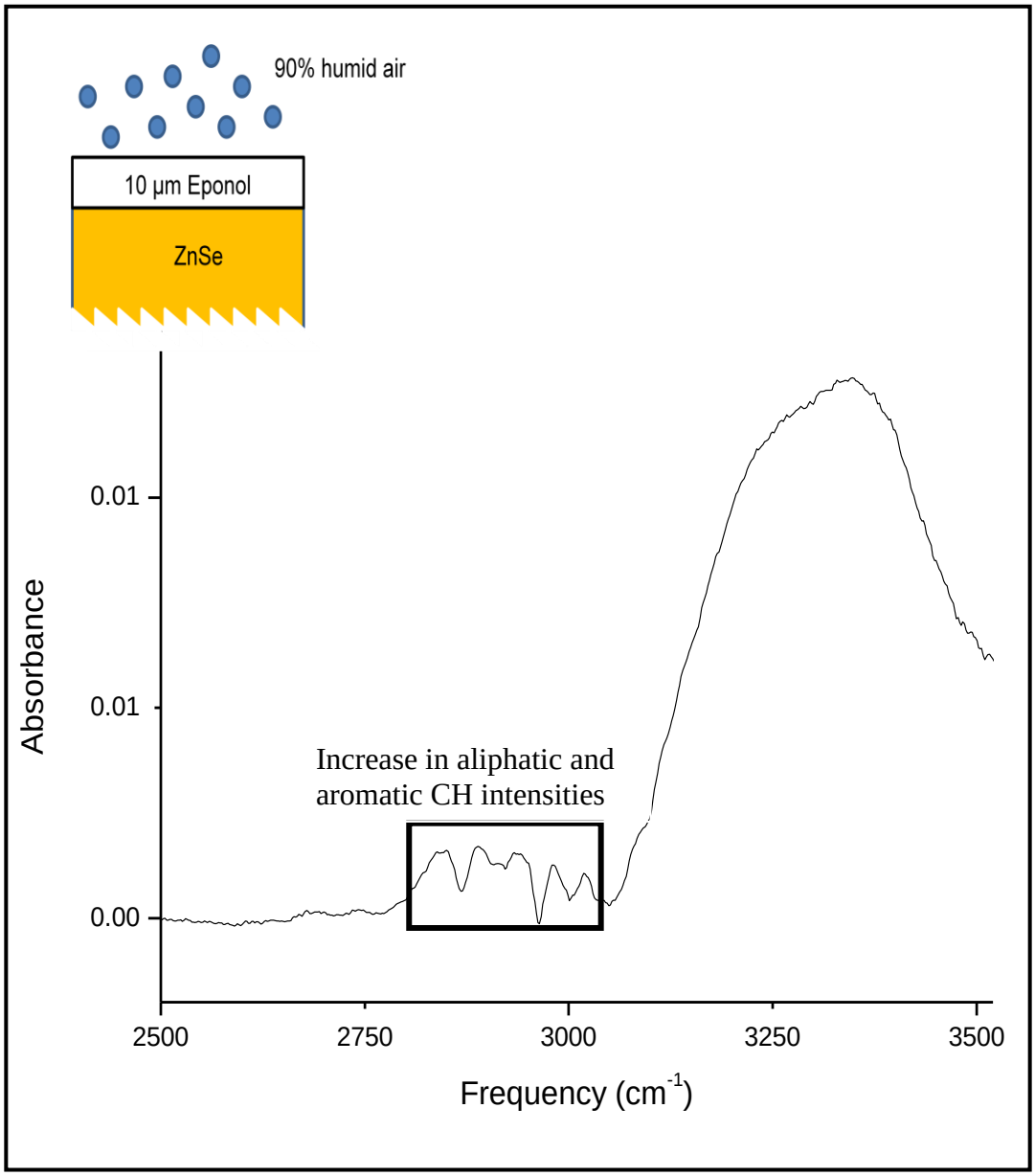

Figure 4.13.ATR-FTIR spectrum of eponol spin coated on ZnSe and exposed to 90% humid air for 20 hours, using the dry sample before exposure as the background. The spectrum is averaged over 400 scans.

Chapter 5

CONCLUSIONS AND RECOMMENDATIONS

With the ever increasing use of organic polymers as high performance coatings for corrosion protection of metal structures that are ubiquitous today, it is extremely important to evaluate the response of these resins to a host of environmental agents to which these adhesively bonded structures are constantly exposed in day to day life. Understanding the degradation mechanisms of these polymers has become integral in designing improved coating systems for a wide array of environments. The polymer/metal interface is the most sensitive region, being extremely fragile in nature and any detrimental changes in this zone will cause the structure to deteriorate via delamination of the polymer from the metal surface.

In the first part of this study, Poly (vinyl butyral-*co*-vinyl alcohol-*co*-vinyl acetate) was used as the test polymer, whose degradation upon exposure to ozone, humidity and UV-B radiation was assessed employing Attenuated Total Reflection Fourier Transform Infrared (ATR-FTIR) spectroscopy. The polymer was found to structurally degrade when exposed to 0.1 ppm ozone, 90% humidity and UV-B light as evident from the formation of carbonyl products, which proceeds via ring opening and chain scission. Also, the exposed PVB showed a much greater water uptake reaching

saturation within a very short time compared to its unexposed counterpart. Interestingly, there was no sign of structural degradation when the polymer was exposed to humidity and UV-B alone, without the ozone. This proves that ozone (or rather atomic oxygen formed from ozone) is required for structural deterioration of the polymer. These changes were detected at a few nanometers from the PVB-ZnSe interface within a 10 μm PVB film.

In the second part of the thesis, the response of an aluminum-PVB interface to liquid water was studied in situ over time using ATR-FTIR spectroscopy. The interface was formed between a 10 μm PVB film spin coated on a 50 nm aluminum film. From the relevant ATR-FTIR spectra, water was found to be incorporated at the interface leading to swelling and delamination of the polymer from the aluminum surface. Corrosion products (aluminum oxide/hydroxide) were also seen to form at the interfacial region. The aluminum-PVB interface was also found to retain water at the interface, long after the water on the sample dried. A comparison with an epoxy resin, diglycidyl ether of bisphenol-A also forming an interface with aluminum gave some contrasting results. Although water was still detected at the interface, the C-H intensities were seen to increase. It was discussed [*in chapter 4*], that this is probably due to a rearrangement of the macromolecular polymer chains upon interaction with water. Corrosion products were seen to form within the first hour of exposure and remained constant throughout the remaining time.

This study is an attempt to gain a better understanding of polymer degradation and the stability of polymer-metal interfaces, representing a key to improve the durability

of adhesively bonded structures. However, extensive research is required to gain a thorough insight into the physical and chemical mechanisms responsible for the failure of coatings. Quantification of such degradation employing appropriate mathematical models would be equally helpful. For example, a useful study can be the quantification of the absorption band at 1580 cm^{-1} observed when a PVB film is exposed to ozone, humidity and UV-B radiation [*Chapter 3*] that would give us the total amount of carboxylate moieties (oxidized carbon) generated due to the degradation. Again, it would be interesting to understand the extent of damage in the bulk of the polymer using transmission FTIR spectroscopy, in tandem with the interfaces. A comparison between the two would help understand the extent of impact at different depths of the polymer film which may shed light on the mechanistic aspects of such degradation. Moreover, the approach should be extended to multilayer structures of polymers and other aggressive media like SO_2, NO_x and temperature cycling. Finally, these laboratory exposed samples should be compared to field samples for lifetime predictions of coating formulation.

REFERENCES

1. http://www.corrosion-doctors.org/Principles/Cost.htm (last visited on 11-4-2010)

2. Sorensen, P.A., Kiil, S., Dam-Johansen, K., Weinell, C.E., Anticorrosive coatings: a review. J. Coat. Technol. Res., 6 (2) 135-176, 2009

3. Fragata, F., Salai, R.P., Amorim, C., Almeida, E., Compatibility and incompatibility in anticorrosive painting The particular case of maintenance painting. Progress in Organic Coatings 56 (2006) 257-268

4. Deflorian, F., Rossi, S., Fedel, M., Organic coatings degradation: Comparison between natural and artificial weathering. Corrosion Science 50 (2008) 2360-2366

5. Fedrizzi, L., Bergo, A., Fanicchia, M., Evaluation of accelerated aging procedures of painted galvanised steels by EIS. Electrochimica Acta 51 (2006) 1864-1872

6. Hare, C.H., Mechanisms of photolytically induced degradation. Coating system design Inc., JPCL March 2003

7. Finlayson-Pitts, B.J., Pitts, Jr., J.N., Chemistry of the Upper and Lower Atmosphere Theory, Experiments and Applications. AP Academic Press, 2000, San Diego, California, USA, ISBN 0-12-257060-X

8. Pospisil, J., Nespurek, S., Photostabilization of coatings. Mechanisms and performance. Prog. Polym. Sci. 25 (2000) 1261-1335

9. Perrin, F.X., Irigoyen, M., Aragon, E., Vernet, J.L., Artificial aging of acrylurethane and alkyd paints: a micro-ATR spectroscopic study. Polymer degradation and stability 70 (2000) 469-475

10. Allen, N.S., Parker, M.J., Regan, C.J., The durability of water-borne acrylic coatings. Polymer degradation and stability 47 (1995) 117-127

11. Lin, S.C., Bulkin, B.J., Pearce, E.M., Epoxy Resins. III. Application of Fourier Transform IR to Degradation Studies of Epoxy Systems. Journal of Polymer Science: Polymer Chemistry Edition, Vol. 17, 3121-3148 (1979)

12. Malanowski, P., Huijser, S., van Benthem, R.A.T.M., van der Ven, L.G.J., Laven, J., de With, G., Photodegradation of poly(neopentyl isophthalate) part I: Laboratory and outdoor conditions. Polymer degradation and stability 94 (2009) 2086-2094

13. Martin, J.W., Nguyen, T., Byrd, E., Dickens, B., Embree, N., Relating laboratory and outdoor exposures of acrylic melamine coatings I. Cumulative damage model and laboratory exposure apparatus. Polymer degradation and stability 75 (2002) 193-210

14. Andrady, A.L., Hamid, S.H., Hu, X., Torikai, A., Effects of increased solar ultraviolet radiation on materials. Journal of Photochemistry and Photobiology B: 46 (1998) 96-103

15. http://www.ucar.edu/learn/1_7_1.htm (last accessed on 11-4-2010)

16. http://web.archive.org/web/20080311005238/http://homeimprovement.superpages.com/painting/do-i-need-to-use-paint-primer.html (last accessed on 11-4-2010)

17. http://www.motochem.com/cp_06/PVB_Polyvinyl_Butyral.htm (last accessed on 11-4-2010)

18. Fernandes M.D., Fernandes, M.J., Hoces, P., Synthesis of Poly(Vinyl Butyral)s in Homogenous Phase and Their Thermal Properties. Journal of Applied Polymer Science, Vol. 102, 5007-5017 (2006)

19. http://en.wikipedia.org/wiki/Polyvinyl_butyral (last accessed on 11-4-2010)

20. Safy El-Din, N.M., Sabaa, M.W., Thermal degradation of poly(vinyl butyral) laminated safety glass. Polymer degradation and stability 47 (1995) 283-288

21. Liau, L.C.K., Tung, M., Kinetic Investigation of Photocatalytic Effects on Poly(vinyl butyral) Photodegradation. Ind. Eng. Chem. Res. 2006, 45, 2199-2205

22. Ohman, M., Persson, D., Leygraf, C., In situ ATR-FTIR studies of the aluminium/polymer interface upon exposure to water and electrolyte. Progress in Organic Coatings 57 (2006) 78-88

23. Lee, L.H., Molecular Bonding and Adhesion at Polymer-Metal Interphases. J. Adhesion, 1994, Vol. 46, pp. 15-38

24. Venables, J.D., Review Adhesion and durability of metal-polymer bonds. Journal of Materials Science 19 (1984) 2431-2453

25. http://www.roymech.co.uk/Useful_Tables/Adhesives/Adhesive_Bond.html (last accessed on 11-4-2010)

26. http://www.rsc.org/ebooks/archive/free/BK9780854045433/BK9780854045433-00001.pdf, Chapter 1 Introduction to Adhesion and Adhesives (last accessed on 11-4-2010)

27. Nguyen, T., Byrd, E., Lin, C., A spectroscopic technique for in situ measurement of water at the coating/metal interface. J. Adhesion Sci. Technol. Vol. 5, No. 9, pp. 697-709 (1991)..

28. Berger, C.M., Henderson, C.L., The effect of humidity on water sorption in photoresist polymer thin films. Polymer 44 (2003) 2101-2108

29. Sangaj, N.S., Malshe, V.C., Review Permeability of polymers in protective organic coatings. Progress in Organic Coatings 50 (2004) 28-39

30. Leygraf, C., Graedel, T.E., Atmospheric Corrosion. Electrochemical Society Series, John Wiley and Sons, Inc., New York, USA, 2000, ISBN 0-471-37219-6

31. Ohman, M., Persson, D., An integrated in situ ATR-FTIR and EIS set-up to study buried metal-polymer interfaces exposed to an electrolyte solution. Electrochimica Acta 52 (2007) 5159-5171

32. Thijs, H.M.L., Remzi Becer, C., Guerrero-Sanchez, C., Fournier, D., Hoogenboom, R., Schubert, U.S., Water uptake of hydrophilic polymers determined by a thermal gravimetric analyzer with a controlled humidity chamber. J. Mater. Chem., 2007, 17, 4864-4871

33. Hu, D.S.G., Chou, K.J.N., Kinetics of water swelling and development of porous structure in ionic poly(acrylonitrile-acrylamide-acrylic acid) hydrogels. Polymer Vol. 37 No.6, pp 1019-1025, 1996

34. McIntyre, J.M., Pham, H.Q., Electrochemical impedance spectroscopy; a tool for organic coatings optimizations. Progress in organic coatings 27 (1996) 201-207.

35. Posner, R., Giza, G., Vlasak, R., Grundmeier, G., In situ electrochemical Scanning Kelvin Probe Blister-Test studies of the de-adhesion kinetics at polymer/zinc oxide/zinc interfaces. Electrochimica Acta 54 (2009) 4837-4843.

36. Nazarov, A.P., Thierry, D., Scanning Kelvin probe studies of metal/polymer interfaces. Electrochimica Acta 49 (2004) 2955-2964.

37. Hajatdoost, S., Sammon, C., Yarwood, J., FTIR-ATR studies of diffusion and perturbation of water in polyelectrolyte thin films. Part 4. Diffusion, perturbation and swelling processes for ionic solutions in SPEES/PES membranes. Polymer (43) 2002 1821-1827.

38. Mura, C., Yarwood, J., Swart, R., Hodge, D., Infrared-ATR studies of the hydration and dehydration of formulated PVC films. Polymer (42) 2001 4141-4152.

39. Ohman, M., Persson, D., Leygraf, C., A Spectroelectrochemical Study of Metal/Polymer Interfaces by Simultaneous In Situ ATR-FTIR and EIS. Electrochemical and Solid-State Letters 10 (4) C27-C30 (2007).

40. Nguyen, T., Byrd, E., Bentz, D., Lin, C., In situ measurement of water at the organic coating/substrate interface. Progress in Organic Coatings 27 (1996) 181-193.

41. Mirabella, F.M., Modern Techniques in Applied Molecular Spectroscopy. John Wiley & Sons, Inc. New York, USA, 1998, ISBN 0-471-12359-5.

42. http://las.perkinelmer.com/content/technicalinfo/tch_ftiratr.pdf (last accessed on 11-4-2010)

43. http://www.piketech.com/technical/application-pdfs/ATR_Theory_andApplication.pdf#zoom=100% (last accessed on 11-4-2010)

44. Philippe, L., Sammon, C., Lyon, S.B., Yarwood, J., An FTIR/ATR in situ study of sorption and transport in corrosion protective organic coatings I. Water sorption and the role of inhibitor ions. Progress in Organic Coatings 49 (2004) 302-314.

45. Fieldson, G.T., Barbari, T.A., The use of FTi.r.-a.t.r spectroscopy to characterize penetrant diffusion in polymers. Polymer, 1993, Volume 34, Number 6.

46. www.refractiveindex.info (last accessed on 11-4-2010)

47. http://www.texloc.com/closet/cl_refractiveindex.html (last accessed on 11-4-2010)

48. http://www.chemicalbook.com/ChemicalProductProperty_EN_CB3749115.htm (last accessed on 11-4-2010)

49. Mattox, D.M., Handbook of physical vapor deposition (PVD) processing. Film formation, adhesion, surface preparation and contamination control. http://books.google.com

50. Zhigal'skii, G.P., Jones, P.K., The physical properties of thin metal films. Taylor & Francis Inc., New York, USA, 2003, ISBN 0-415-28390-6.

51. Zhang, Y., Ding, Y., Li, Y., Gao, J., Yang, J., Synthesis and characterization of polyvinyl butyral – $Al(NO_3)_3$ composite sol used for alumina based fibers. J Sol-Gel Sci Technol (2009) 49: 385-390.

52. Scatena, L.F, Brown, M.G., Richmond, G.L., Water at Hydrophobic Surfaces: Weak Hydrogen Bonding and Strong Orientation Effects. Science 292, 908 (2001)

53. Vlasak, R., Klueppel, I., Grundmeier, G., Combined EIS and FTIR-ATR study of water uptake and diffusion in polymer films on semiconducting electrodes. Electrochimica Acta 52 (2007) 8075-8080.

54. Liau, L.C.K., Yang, T.C.K., Viswanath, D.S., Mechanism of Degradation of Poly(vinyl butyral) Using Thermogravimetry/Fourier Transform Infrared Spectroscopy. Polymer Engineering and Science, November 1996, Vol. 36, No. 21, 2589-2600

55. Silverstein, R.M., Webster, F.X., Kiemble, D.J., Spectrometric identification of organic compounds, Seventh Edition. John Wiley & Sons, Inc., 2005, New Jersey, USA, ISBN 978-0-471-39362-7.

56. Gu, X., Stanley, D., Byrd, W.E., Dickens, B., Vaca-Trigo, I., Meeker, W.Q., Nguyen, T., Chin, J.W., Martin, J.W., Linking Accelerated Laboratory Test with Outdoor Performance Results for a Model Epoxy Coating System. Service Life Predictions of Polymeric Materials, 2009, Part I, 3-28, DOI: 10.1007/978-0-387-84876-1_1

57. Reinohl, V., Sedlart, J., Navratil, M., Photo-oxidation of Poly(vinyl butyral). Polymer Photochemistry 1 (1981) 165-175

58. Liu, R., He, B., Chen, X., Degradation of Poly(vinyl butyral) and its stabilization by bases. Polymer Degradation and Stability 93 (2008) 846-853.

59. Liau, L.C.K., Yang, T.C.K., Viswanath, D.S., Reaction Pathways and Kinetic Analysis of PVB Thermal Degradation Using TG/FT-IR. Applied Spectroscopy, Volume 50, No. 8, 1996, 1058-1065

60. Phambu, N., Characterization of aluminum hydroxide thin film on metallic aluminum powder. Materials Letters, Volume 57, Issue 19, 2003, Pages 2907-2913.

61. Ping, Z.H., Nguyen, Q.T., Chen, S.M., Zhou, J.Q., Ding, Y.D., States of water in different hydrophilic polymers – DSC and FTIR studies. Polymer 42 (2001) 8461-8467.

62. Liu, D., Ma, G., Levering, L.M., Allen, H.C., Vibrational Spectroscopy of Aqueous Sodium Halide Solutions and Air-Liquid Interfaces. Observation of Interfacial Liquid Depth. J. Phys. Chem. B. 2004, 108, 2252-2260.

63. Sammon, C., Mura, C., Yarwood, J., Everall, N., Swart, R., Hodge, D., FTIR-ATR Studies of the Structure and Dynamics of Water Molecules in Polymeric Matrices. A Comparison of PET and PVC. J. Phys. Chem. B. 1998, 102, 3402-3411.

64. Alexander, M.R., Thompson, G.E., Beamson, G., Characterization of the oxide/hydroxide surface of aluminum using x-ray photoelectron spectroscopy: a procedure for curve fitting the O 1s core level. Surf. Interface Anal. 29, 468-477 (2000).

65. Jeurgens, L.P.H., Sloof, W.G., Tichelaar, F.D., Borsboom, C.G., Mittemeijer, E.J., Determination of thickness and composition of aluminum-oxide overlayers on aluminum substrates. Applied Surface Science 144-145 (1999) 11-15.

66. Stralin, A., Hjertberg, T., Influence of surface composition on initial hydration of aluminum in boiling water. Applied Surface Science 74 (1994) 263-275.

67. Van Gils, S., Melendres, C.A., Terryn, H., Quantitative chemical composition of thin films with infrared spectroscopic ellipsometry: applications to hydrated oxide films on aluminum. Surf. Interface Anal. 2003; 35: 387-394.

68. Dickie, S.A., Mcquillan, A.J., In-Situ Infrared Spectroscopic Studies of Adsorption Processes on Boehmite Particle Films: Exchange of Surface Hydroxyl Groups Observed upon Chelation with Acetylacetone. Langmuir 2004, 20, 11360-11636.

69. Wicks Jr., Z.W., Jones, F.N., Pappas, S.P., Wicks, D.A., Organic Coatings Science and Technology Third Edition. John Wiley & Sons Inc., New Jersey, USA, 2007, ISBN 978-0-471-69806-7.

70. Khanna, A.S., High-performance organic coatings. CRC Press LLC, Florida, USA 2008. ISBN 978-1-4200-7969-2.